Journal of Structural Geology 195 (2025) 105391

Contents lists available at ScienceDirect

Journal of Structural Geology

journal homepage: www.elsevier.com/locate/jsg

Characteristics and modelling of slip-rate variability and temporal earthquake clustering across a distributed network of active normal faults constrained by *in situ* ^{36}Cl cosmogenic dating of fault scarp exhumation, central Italy

Roberts G.P [a,*], Iezzi F [b], Sgambato C [a], Robertson J [a], Beck J [c], Mildon Z.K [d], Papanikolaou I [e], Michetti A.M [f,n], Faure Walker J.P [g], Mitchell S [a], Meschis M [h], Shanks R [i], Phillips R [j], McCaffrey K.J.W [k], Vittori E [l], Visini F [m], Iqbal M [a]

[a] Birkbeck, University of London, WC1E 7HX, UK
[b] Department of Earth Sciences, Environment and Resources (DiSTAR), University Federico II, Naples, Italy
[c] Center for Integrative Petroleum Research (CIPR),CPG, King Fahd University of Petroleum and Minerals, Saudi Arabia
[d] School of Geography, Earth and Environmental Sciences, University of Plymouth, Drakes Circus, PL4 8AA, UK
[e] Agricultural University of Athens, Greece
[f] Università Degli Studi Dell'Insubria, Via Valleggio 11, 22100, Como, Italy
[g] University College London, Gower Street, WC1E 6BT, UK
[h] Istituto Nazionale di Geofisica e Vulcanologia, Sezione di Palermo, Via Ugo La Malfa, 153, 90146, Palermo, Italy
[i] Scottish Universities Environmental Research Centre, Glasgow, G75 0QF, UK
[j] University of Leeds, School of Earth & Environment, Leeds, LS2 9JT, UK
[k] University of Durham, UK
[l] IGG-CNR Florence, Italy
[m] Istituto Nazionale di Geofisica e Vulcanologia, Sezione di Chieti, Chieti, Italy
[n] Istituto Nazionale di Geofisica e Vulcanologia, Sezione di Napoli Osservatorio Vesuviano, 80100, Napoli, Italy

ABSTRACT

We present a compilation of new and unpublished *in situ* ^{36}Cl cosmogenic isotope data recording the exhumation of 27 active normal fault planes by earthquake slip for the central Apennines, Italy. We do this to constrain the characteristics of slip-rate variability and temporal earthquake clustering and anticlustering across the entire extending orogen, and to assess why it occurs. From the ^{36}Cl observations we report(1) the long-term slip-rates averaged since 20 ka, (2) the percentage of sites with clusters and anticlusters in each 1 kyrs time-slice back to 20 ka, (3) regional maps showing cluster locations for every 1 kyr time-slice, (4) cluster and anticluster durations, and (5) the amounts of slip and slip-rates averaged over the duration of clusters and anticlusters. To study why this slip-rate variability has developed we conduct modelling of stress interactions between faults and underlying shear-zones, and between neighbouring fault/shear-zone structures. We show that the measured slip-rate variability and temporal clustering can be replicated by a model where the transfer of differential stress between faults and their underlying shear-zones, and between neighbouring fault/shear-zone structures, produces changes in strain-rates on underlying viscous shear-zones which drive periods of rapid or reduced slip-rate on their overlying faults. We suggest that stress and hence strain-rate increase on an underlying shear-zone produced by coseismic slip on its overlying fault is the mechanism that initiates an earthquake cluster. Clusters progress because the increased strain-rate on the shear-zone reloads the overlying fault producing a positive feedback loop. The clusters also produce stress reduction on fault/shear-zones located across strike, initiating anticlusters in those locations. The durations of anticlusters will be set by the summed coseismic and interseismic stress changes through time, because although these shear-zones develop relatively low viscous strain-rates, eventually they will load their overlying fault to failure initiating a new cluster. These interactions cause the locations of clusters and anticlusters to migrate across and along-strike within the fault system. Such constraints on the processes producing clustering and anticlustering should allow observations of these phenomena to be included in probabilistic seismic hazard assessments (PSHA), and interpretations of the rheology of deforming continental crust.

* Corresponding author.
E-mail address: g.roberts@bbk.ac.uk (R. G.P).

https://doi.org/10.1016/j.jsg.2025.105391
Received 15 August 2024; Received in revised form 31 January 2025; Accepted 28 February 2025
Available online 2 March 2025
0191-8141/

1. Introduction

It is well-known that large magnitude surface faulting earthquakes cluster in time due a growing body of seismological, historical and palaeoseismic data (e.g., Coppersmith, 1988; Sieh et al., 1989; Marco et al., 1996; Rockwell et al., 2000; Klinger et al., 2000; Dawson et al., 2003; Dolan et al., 2007; Oskin et al., 2008; Ganev et al., 2010; Scholz, 2010; Gold and Cowgill, 2011; Grapes and Holdgate, 2014; Clark et al., 2017; Klinger et al., 2015; Dolan et al., 2016; DuRoss et al., 2016; Lefevre et al., 2018; Verdecchia et al., 2018; Wechsler et al., 2018; Angster et al., 2019; Cooke et al., 2020; Hatem et al., 2021; Iezzi et al., 2021; Elston et al., 2022; Mildon et al., 2022; Zygouri et al., 2023; Roberts et al., 2024; Dolan et al., 2024). Several large magnitude surface faulting earthquakes can occur within relatively short periods of time separated by longer time periods where the fault appears to be relatively dormant with few or no large magnitude surface faulting events. This clustering and anticlustering of large magnitude surface faulting earthquakes, and presumably also smaller magnitude earthquakes defined by the b-value for individual faults, is associated with temporal and spatial slip-rate variability (e.g. Cowie et al., 2007; Cowie et al., 2012; Pace et al., 2016; Dolan et al., 2024).

It is also well-known that networks of brittle active faults with underlying viscous shear-zones exist in deforming regions, with individual fault/shear-zone structures working together to produce the regional deformation due to stress interactions (Peach et al., 1888; Savage and Burford, 1973; Sibson, 1977; White et al., 1980; Schmid, 1982; Reston, 1990; King et al., 1994; England and Molnar, 1997; Boncio et al., 1998; Hirth et al., 2001; Stein, 2003; Ellis and Stöckhert, 2004; Cowie et al., 2005; Trepmann et al., 2007; Shimamoto and Noda, 2014; Moore and Parsons, 2015; Cowie et al., 2013; Allison and Dunham, 2018; Mildon et al., 2022; Roberts et al., 2024). It is therefore desirable to understand how the slip-rate variability and temporal earthquake clustering relates to the interaction between faults and shear-zones because this may be the key to understanding how to interpret regional strain-rate patterns in terms of the mechanics of continental deformation (England and McKenzie, 1982; England and Molnar, 1997; Sonder and England, 1989; Cowie et al., 2005; Faure Walker et al., 2012; Cowie et al., 2013), and in terms of the geography of seismic hazard (Pace et al., 2014; Valentini et al., 2017). Unfortunately, we lack this capability because there is a sparsity of datasets that constrain the spatial patterns and temporal variability of fault and shear-zone activity across entire deforming orogens (Dolan et al., 2024). This means it is challenging to assess how faults and shear-zones, and networks of active fault/shear-zone structures interact over time periods long-enough to have multiple large magnitude surface faulting earthquakes on every fault in the system.

The objectives of this paper are to (1) to provide a database that defines slip-rate variability alongside clustering and anticlustering of large magnitude surface faulting earthquakes for most major faults in a region of extension in the central Apennines, Italy, and (2) use this database to see how temporal and spatial patterns of surface slip relate to the interaction between faults and shear-zones because this may be the key to understanding how to interpret regional strain-rate patterns in terms of the mechanics of continental deformation. We present a dataset for central Italy of slip versus time for 27 sites along active normal fault/shear-zones, 12 of which have not been previously published, and these along with an additional 6 previously-published sites have not been modelled previously with the code presented by Beck et al. (2018). We recover this record of slip through modelling of 479 determinations of the *in situ* ^{36}Cl cosmogenic isotopic concentrations of carbonate rock samples from the fault planes exposed due to surface faulting produced by large magnitude (Mw 6.0–7.0) earthquakes. The dataset constrains the slip across many of the main faults in the region over a continuous time-period of at least 20 kyrs. We document slip-rate variability and temporal earthquake clustering on individual faults, and hence across the whole network of faults. Building on existing papers that only individually studied <6 faults (Mildon et al., 2022; Roberts et al., 2024), we quantify the characteristics of the regional patterns of earthquake clustering across 27 sites on 26 faults such as (1) the number of faults experiencing surface slip in each 1 kyrs time slice, (2) the durations of clusters and anticlusters, (3) the amounts of surface slip in clusters and anticlusters, and (4) how much the slip-rate in clusters and anticlusters is increased or decreased relative to the long-term slip-rate. We discuss the processes that may control clustering such as (a) dynamic topography, (b) stress interactions between faults and their underlying shear-zones, and between neighbouring fault/shear-zone structures, (c) microstructural annealing, (d) fluid involvement, and (e) failure related to rate-and-state friction. We discuss what understanding of the causes of clustering would imply for (i) the historical record of earthquakes in a region, (ii) geodetic constraints of the regional strain-rates measured over the last few decades, (iii) the rheology of deforming continental crust, and (iv) probabilistic seismic hazard assessment.

2. Conceptual background

It has been shown that it is possible to recover exhumation versus time histories on active normal faults from *in situ* ^{36}Cl cosmogenic isotopic concentrations of carbonate rock samples from the fault planes (Mitchell et al., 2001; Benedetti et al., 2002, 2003, 2013; Palumbo et al., 2004; Schlagenhauf et al., 2010, 2011; Cowie et al., 2017; Beck et al., 2018; Mechernich et al. 2018, 2023; Mozafari et al. 2019, 2021; Tesson and Benedetti, 2019; Tikhomirov et al., 2019; Goodall et al., 2021; Iezzi et al., 2021; Mildon et al., 2022; Roberts et al., 2024). These exhumation histories can be interpreted as earthquake slip versus time if sample sites are carefully selected to exclude exhumation/burial of the fault planes due to erosion and sedimentation (Bubeck et al., 2015; Cowie et al., 2017). The derived slip histories are characterised by periods of rapid slip that must contain temporal clusters of surface faulting earthquakes because the slip increases of, for example, 7 m in only 1.25 kyrs are too large to explain with a single earthquake (Mildon et al., 2022; Roberts et al., 2024). The clusters are separated by low slip-rate periods, with little or no slip, where few or no surface faulting earthquakes can have occurred, and these time periods are termed anticlusters. The clusters occur at different times on neighbouring across-strike faults (Mildon et al., 2022; Roberts et al., 2024). This out-of-phase slip has been explained by stress interactions between faults and their underlying shear-zones, combined with stress interactions between neighbouring across-strike fault/shear-zone structures. The idea is that slip in a cluster decreases the differential stress on shear-zones located across strike reducing their viscous strain-rates. The magnitude of the strain-rate decreases implied by a typical viscous flow law for the mid to lower crust (e.g. Hirth et al., 2001), match those measured on their overlying brittle fault using ^{36}Cl data. The use of the viscous flow law for dislocation creep in quartz from Hirth et al. (2001), is an assumption, because the composition of the mid and lower crust can be uncertain. However, given the typical quartz-rich granitic to granodioritic composition of the upper crust, and the quartz-rich tonalitic composition of the bulk continental crust (Wedepohl, 1995), the assumption that dislocation creep in quartz plays a major role in the rheology of continental crust may be the most appropriate starting point. The relationship between differential stress changes and strain-rate variations is explained in Fig. 1a which shows a hypothetical network of 35 normal faults and the upper portions of their underlying shear-zones. Changes in differential stress have been calculated using the *Coulomb 3.4* software across four Mw 6.6 earthquakes on fault eighteen, with 1 m coseismic slip at the surface, and with a recurrence interval of 1000 years (slip rate = 1 mm/yr), plus interseismic loading from slip on the shear-zone beneath fault eighteen at rate that would produce 1 mm/yr of slip on the overlying fault (Mildon et al., 2022; figure adapted from Roberts et al., 2024). The Coulomb stresses have been converted to differential stresses using the relations shown in King et al. (1994) (see Mildon et al., 2022 for a full explanation). Changes in differential stress on receiver fault/shear-zones are relatively large, and of particular interest are the stress changes for the

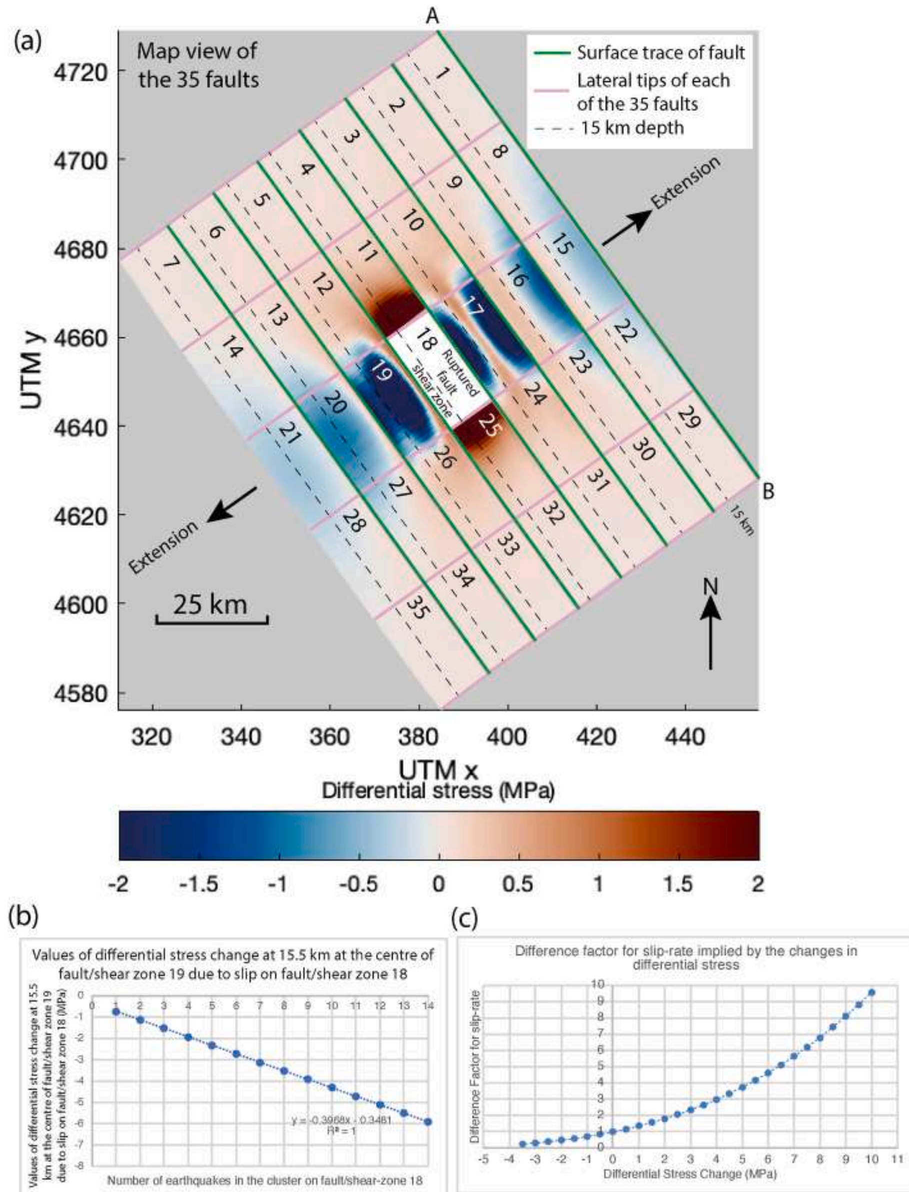

Fig. 1. Stress transfer concept. Cumulative differential stress changes across a grid of 35 normal fault/shear-zones, each with a dip of 60°, given (i) four Mw 6.6 earthquakes on fault eighteen (each with 1 m coseismic slip at the surface) with a recurrence interval of 1000 years, and (ii) interseismic loading from the shear-zone beneath fault eighteen at rate that would produce 1 mm/yr of slip on the overlying fault. (a) Map view of the faults at depth assuming a transparent crust. (b) Calculated values of differential stress change at 15.5 km depth for the centre of the fault trace of fault nineteen, given between 1 and 8 earthquakes on fault eighteen, again with 1 m slip at the surface and a recurrence interval of 1000 years within the earthquake cluster. (c) Implied changes in slip-rate given the stress changes in (b). Overall, this figure implies that the slip-rate reduction on any of the faults due to a cluster can be calculated given inputs on the kinematics, magnitudes of slip, and geometry of the fault system.

viscous shear-zones because it is well-known that such stress changes alter the strain-rates within viscous shear-zones. This is because strain-rate, $\dot{\varepsilon}$, and differential stress, σ, are related by the general form $\dot{\varepsilon} \propto \sigma^n$, with $n = \sim 3$ (Hirth et al., 2001). In this paper we use the quartz flow law for dislocation creep in quartz (Equation (1)), where, $\dot{\varepsilon}$ is strain rate, A is a material parameter, fH_2O is water fugacity, m is the water fugacity exponent, σ is the differential stress, n is the stress exponent, Q is the activation energy, R is the ideal gas constant, and T is absolute temperature.

$$\dot{\varepsilon} = AfH_2O^m(\sigma_1 - \sigma_3)^n \exp(-Q/RT) \quad (1)$$

Values we use as variables in equation (1) are the same as those in Mildon et al. (2022). Using this flow law, the differential stress changes in Fig. 1a imply changes in strain-rate associated with the fault/shear-zones, which have been displayed as changes in slip-rate (Fig. 1b and c). Slip-rates on the brittle faults are calculated by assuming conservation of heave across the dipping shear-zones and overlying faults, conserving strain compatibility with depth. Slip-rates can be doubled or halved compared to the long-term slip-rate by changes in differential stress of +2.5 or −2.5 MPa. Stress changes with similar magnitudes to those shown in Fig. 1 have been calculated for periods of fluctuating slip-rate implied by ^{36}Cl data for active normal faults in central Italy, and the predicted slip-rate changes match those implied by the ^{36}Cl data (Mildon et al., 2022; Roberts et al., 2024). These authors deliberately excluded modelling of spatio-temporal variability in frictional properties, and effective stresses due fluid flow within heterogeneous rock masses to focus on whether changes in differential stress alone could reproduce the observed values of slip-rate variation recorded by ^{36}Cl data. They argued that because calculated strain-rate and slip-rate changes on fault-shear-zones replicate those recorded by ^{36}Cl data, stress interactions between faults and their underlying shear-zones, and stress interactions between neighbouring fault/shear-zone structures, could be the 1st order explanation for temporal earthquake clustering in these examples. The question that emerges, that we explore in this paper, is whether the characteristics of temporal clustering across entire extending regions of continental crust, with complex across-strike and along-strike stress interactions, can be explained in the same way. To test this hypothesis, a dataset detailing slip through time on multiple faults across the entire width of an extending region are required, and we provide this herein.

3. Geological background

The Italian Apennines (Figs. 2 and 3) provide an opportunity to investigate the characteristics of temporal earthquake clustering across an entire extending region. This is because a network of active normal faults is well exposed, with carbonate fault planes on many of the major faults that have been exhumed by earthquake slip over the last few tens of millennia. These features mean that the fault planes are amenable to study with *in situ* ^{36}Cl cosmogenic exposure dating, that in turn can provide slip versus time histories for the faults. Assuming strain compatibility between faults and their underlying shear-zones, slip versus time histories for the faults also constrain strain-rate versus time histories for the underlying shear-zones (Mildon et al., 2022; Roberts et al., 2024).

The region has developed active normal faults in the last ~2–3 Myrs, following previous compressional fold-thrust belt deformation in the early Pliocene and Miocene associated with subduction that has rolled-back towards the east and north-east (Nijman, 1971; Bosi, 1975; Doglioni, 1993; Cello et al., 1997; Selvaggi, 1998; Pialli and Alvarez, 1995; Cavinato and De Celles, 1999; Piccardi et al., 1999; Galadini and Galli, 2000; Tondi, 2000; Galadini and Messina, 2004; Roberts and Michetti, 2004; Maschio et al., 2005; D'Agostino et al., 2011; Vezzani et al., 2010; Gori et al., 2017; Faure Walker et al., 2021; Lavecchia et al., 2022).

Debate exists about how active normal faults at the surface continue to depth and how the active extensional deformation is accommodated in the viscous middle and lower crust. In many places surface geological mapping has shown that active normal faults cut-across pre-existing Alpine-age thrusts and continue to depth (Nijman, 1971; Roberts and Michetti, 2004; Lavecchia et al., 2017), whereas in other cases interpretations of seismic reflection data suggest that active normal faults in the top 10–15 km of the crust either cut across, or merge downwards or abut against pre-existing thrusts or low-angle extensional detachments (Boncio et al., 1998; Barchi et al., 2003; Finetti et al., 2001; Collettini et al., 2006; Brozzetti et al., 2009; Lavecchia et al. 2011, 2017; Mirabella et al., 2011). Thus, complexity exists in the top 10–15 km of the crust with regard to the extensional structures. However, evidence from mainshock and aftershock data from recent Ms 6.2–6.5 earthquakes in 2009 and 2016 suggest that some faults are relatively planar to depths of ~10–15 km (Chiaraluce et al., 2011; Lavecchia et al., 2017; Michele et al., 2020), and the depth of the brittle to viscous transition in central Italy appears to occur at a depth of ~12–15 km (Lavecchia et al., 2017), although it may fluctuate during the seismic cycle (Rolandone et al., 2004). However, it is unclear what the geometries of the deformation are at depths greater than 10–15 km, where higher temperatures and pressures dictate that viscous processes are likely to operate. Roberts et al. (2024), using the observation that mainshock and aftershock data suggest that some faults are relatively planar to depths of ~10–15 km, proposed that underlying shear zones are likely to share similar

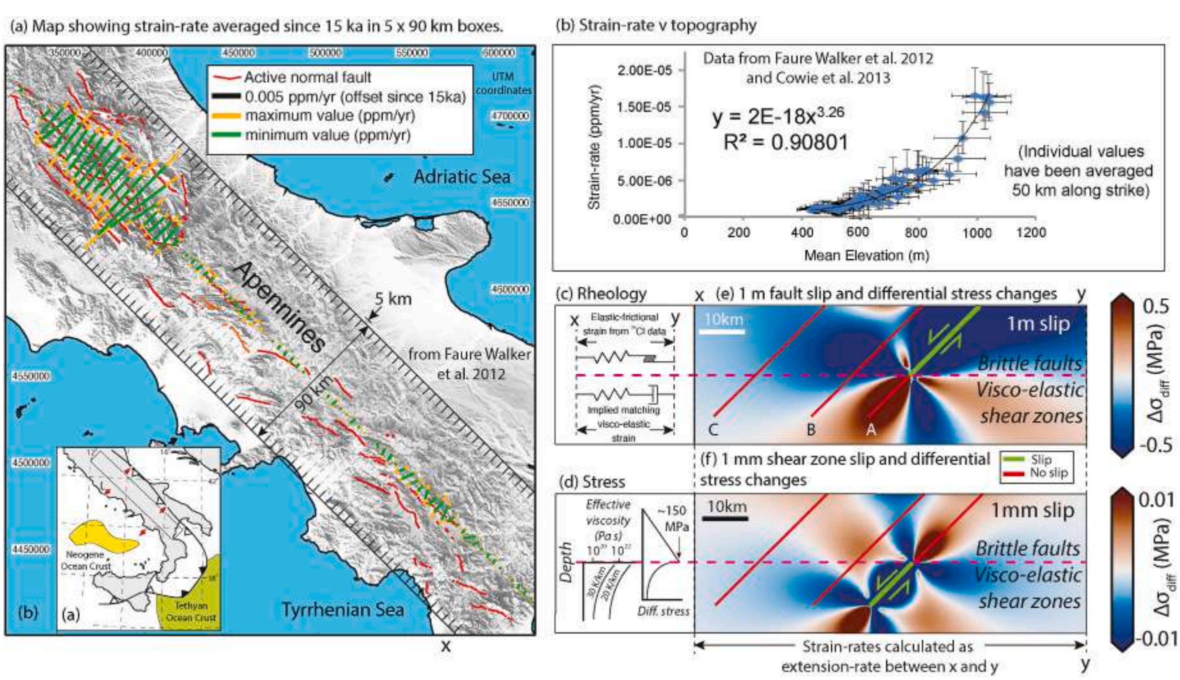

Fig. 2. The relationship between strain-rate and topographic elevation in the Apennines and implications for stress modelling of earthquake clustering (adapted from Faure Walker et al., 2012; Cowie et al., 2013; Mildon et al., 2022; Roberts et al., 2024). (a) Strain-rates averaged since 15 ka from offsets across fault scarps exposed at the surface. Values are calculated across all 5 × 90 km boxes traversing the Apennines. (b) Strain rates from (a) are plotted against average elevations from SRTM data in 5 × 90 km boxes. A power law relationship exists, with an exponent of 3.26. This resembles the power-law relationship for dislocation creep, where strain-rate is proportional to differential stress raised to the power n, with n = ~3 (Hirth et al., 2001). Topographic elevation contributes to the vertical stress, implying that it contributes to the differential stress at depth. Slip-rates on the brittle faults are driven by the viscous strain-rates on underlying shear-zones, because the strain-rates are controlled by differences in elevation and hence differential stress in the viscous layer. (c) Brittle-elastic strain in the upper crust (spring and frictional ratchet) is matched by visco-elastic strain at depth (spring and dash-pot) when summed over numerous earthquakes cycles. (d) The differential stress and viscosity changes with depth for a given depth versus temperature regime (after Allison and Dunham, 2018), and stresses produced by slip on a shear-zone.

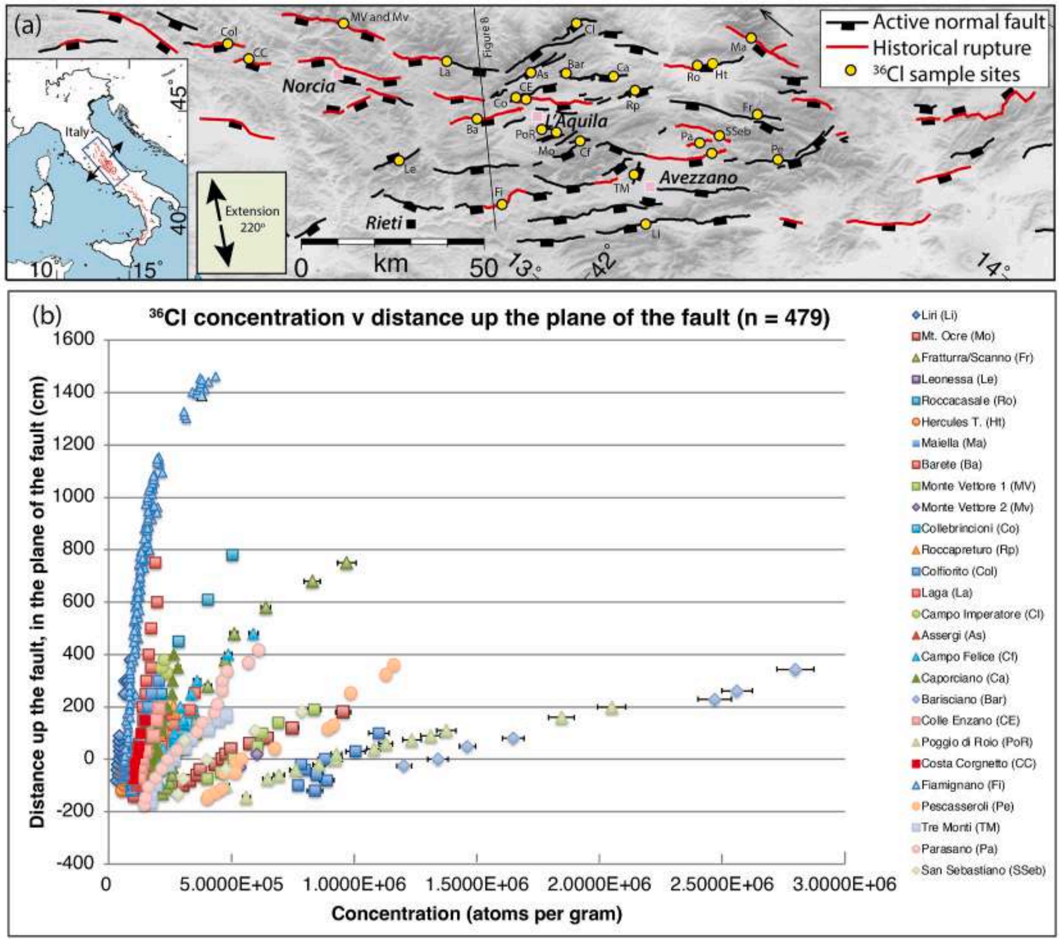

Fig. 3. Sample locations in central Italy and ^{36}Cl concentrations. Line locates the cross-section in Fig. 8.

planar geometries to the brittle normal faults in the upper crust, at least for a few kilometres beneath the brittle-viscous transition, as seen in other well-imaged regions of normal faulting (e.g. Reston, 1990; Phillips et al., 2016). For this paper we have assumed that in the depth range of ~15–20 km shear-zones are likely to exhibit similar dips to their overlying brittle faults.

The present extension rate measured across the region of extension with GPS geodesy is ~3–4 mm/yr (D'Agostino et al., 2011), with similar rates recently confirmed with InSAR (Daout et al., 2023). The extending region, which is mainly within the high topography of the Apennines, experiences destructive normal faulting earthquakes, with many fatalities and injuries, such as the Mw 6.9 1915 Avezzano earthquake, Mw 5.6–6.0 1997 Colfiorito earthquakes, Mw 6.3 2009 L'Aquila earthquake, and the 2016 Mw 6.2–6.6 Amatrice-Norcia earthquakes. These earthquakes all produced surface faulting on bedrock scarps with carbonate fault planes, with surface coseismic slip ranging from a few centimetres up to 2.4 m, implying that such scarps grow through repeated earthquake slip (Serva et al., 1988; Vittori et al., 2000; Emergeo Working Group, 2010; Wilkinson et al., 2017; Iezzi et al., 2021; Villani et al., 2018).

Palaeoseismic results from these faults, derived through trenching and dating of colluvial wedges and event horizons, reveal numerous prehistoric surface faulting earthquakes, with recurrence intervals that are typically hundreds to a few thousand years, with some examples exhibiting non-regular recurrence intervals on individual faults (Galli and Naso, 2009; Cinti et al., 2021). The region has also been investigated with *in situ* ^{36}Cl cosmogenic dating of exhumed carbonate fault planes (Palumbo et al., 2004; Schlagenhauf et al., 2010, 2011; Benedetti et al., 2013; Cowie et al., 2017; Beck et al., 2018; Tesson and Benedetti, 2019; Goodall et al., 2021; Mildon et al., 2022; Roberts et al., 2024). These ^{36}Cl studies have attempted to constrain slip-rates, and in some cases earthquake recurrence for the active faults, but these parameters can only be considered robust for sites that have been shown to be free of erosion and sedimentation during the Holocene and late glacial, because these processes may well have removed material covering the fault planes or buried fault planes in the past affecting ^{36}Cl production and hence the concentrations of ^{36}Cl. This problem has been addressed by Bubeck et al. (2015) and Cowie et al. (2017) who describe how to identify sample sites that will be free of such erosion and sedimentation. Using these criteria, examples now exist where the timing and magnitude of surface slip have been constrained using ^{36}Cl, and these reveal that slip-rates fluctuate through time, but determining the timing of individual earthquakes can be challenging (Benedetti et al., 2013; Cowie et al., 2017; Goodall et al., 2021; Mildon et al., 2022; Roberts et al., 2024). Advances in the modelling of the ^{36}Cl data needed to retrieve slip histories now allows us to account for uncertainties in early ^{36}Cl production by drawing slip from a Brownian Passage Time (BPT) model of earthquake recurrence, slip per event, and uncertainty in ^{36}Cl production parameters using a full Bayesian approach (e.g. Beck et al., 2018). Results using this code show that surface slip is produced by fluctuating periods of relatively rapid slip-rate interspersed with periods of much lower or zero slip-rate lasting many millennia (e.g. Mildon et al., 2022; Roberts et al., 2024). The periods of rapid slip must involve several surface faulting earthquakes because measured slip in these periods is too large to be produced by single earthquakes (Wells and Coppersmith, 1994; Wesnousky, 2008).

Where slip-rate fluctuations derived from ^{36}Cl data have been compared with palaeoseismic results from trenching that constrain the ages colluvial wedges and event horizons, there is, in general, a good agreement in terms of timing of slip episodes. Results show that palaeoearthquake occurrences from trenching tend to fall in the rapid slip periods derived from the ^{36}Cl, with fewer or no palaeoearthquakes in the times of low-slip-rate from ^{36}Cl (Cowie et al., 2017; Mildon et al., 2022; Roberts et al., 2024). However, more work is required to compare slip-rates and exact earthquake timings between these two approaches because (a) in general, only the minimum slip per event, and hence slip-rate, can be gained from trenching studies due to uncertainty in the relationship between the vertical extent of colluvial wedges and the coseismic slip magnitude that produced them, and (b) it can be challenging to gain slip per event for individual earthquakes from ^{36}Cl data, and these authors suggest that ^{36}Cl observations are better suited to constraining slip-rate fluctuations across periods of time that are likely to contain several surface faulting earthquakes rather than individual earthquake timings (see below).

In addition to the excellent exposure of active normal faults, the Italian Apennines also has excellent constraints on the relationship between surface faulting and deformation processes deeper in the crust. Cowie et al. (2013) showed a power law relationship exists between surface elevations and the strain-rates measured across normal faults since the demise of the high erosion rates that typified the Last Glacial Maximum (LGM) at ~15 ± 3 ka. Surface slip produced by earthquakes was produced during the cold climates of the last glaciation, but scarps only become preserved after the demise of the LGM when erosion rates associated with freeze-thaw action declined. The slip across scarps therefore represents the slip since around 15 ± 3 ka, allowing the calculation of slip-rates averaged over this time-period. Elevation values were derived from SRTM data measured within 5 × 90 km boxes arranged across the strike of the Apennines (Fig. 2a). Strain-rates averaged over 15 ± 3 ka were derived by summing slip-rates between all faults that occur within the 5 × 90 km boxes. Elevation and strain-rate data from the 5 × 90 km boxes were averaged along strike in 50 km wide moving sample windows, although other sample windows produced similar results. The resultant correlation between strain-rates and topographic elevation exhibits a power-law relationship where the elevation exponent, n, is equal to ~3.26 (Fig. 1b). This was interpreted by Cowie et al. (2013) by noting that elevation differences contribute to the vertical stress and hence differential stress at depth. Thus, the relationship between elevation and strain-rate resembles the power-law relationship for dislocation creep, where strain-rate, $\dot{\varepsilon}$, and differential stress, σ, are related by $\dot{\varepsilon} \propto \sigma^n$, with $n = \sim 3$ (Hirth et al., 2001) (see above). Thus, in terms of the relationship between surface faulting and deformation processes deeper in the crust, it is implied that the slip-rates on the brittle faults are driven by the viscous strain-rates on underlying shear-zones, because the strain-rates appear to be controlled by differences in elevation and hence differential stress. The identification of viscous processes within shear-zones in controlling the rates of brittle slip on the overlying faults for the Italian Apennines concurs with old, but classic ideas where it has long been thought that faults are underlain by viscous shear-zones that drive the deformation (Savage and Burford, 1973; Sibson, 1977). The question that arises is how to reconcile the long-term strain-rates implied by strain-rates averaged since 15 ± 3 ka (Fig. 2) with observations of fluctuating slip-rate from ^{36}Cl studies of fault planes, and also changes in strain-rate implied by stress transfer calculations when combined with viscous flow laws (Fig. 1).

This question has been addressed for the central Apennines by two previous papers Mildon et al., (2022); Roberts et al., (2024), but with relatively small numbers of studied faults, and limited results. Mildon et al. (2022) studied 6 faults with ^{36}Cl data (the Mt. Vettore, Colfiorito, Leonessa, Laga, Barete and Fiamignano faults). They found a consistent pattern of decreasing differential stress (σ) on postulated receiver shear-zones beneath faults undergoing anticlusters with little or no surface slip lasting several millennia implied by the ^{36}Cl data. The decreasing differential stress was shown to be due to stress transfer produced by periods of rapid slip on neighbouring fault/shear-zones located mainly across strike lasting several millennia, again constrained by ^{36}Cl data on those faults. The modelled magnitudes of these stress decreases on receiver faults was used to calculate implied strain-rate ($\dot{\varepsilon}$) and hence slip-rate decreases on receiver faults using a viscous flow-law for quartz that has the form of $\dot{\varepsilon} \propto \sigma^n$ (see Hirth et al., 2001 and Equation (1) for details of the flow law). They found that the magnitude of the implied strain-rate and hence slip-rate decreases replicated the slip-rate decreases on receiver faults during anticlusters recorded by the ^{36}Cl data. This suggested that strain-rates averaged over 15 ± 3 kyrs driven by long-term patterns of topographic elevation can be modulated by fault/shear-zone interactions lasting a few millennia, partially addressing the question in the previous paragraph. It is only a partial answer because Mildon et al. (2022) did not investigate or explain how the periods of rapid slip (temporal earthquake clusters lasting several millennia) developed on neighbouring fault/shear-zones. To address this, Roberts et al. (2024) studied ^{36}Cl data from 3 faults located across strike from each other in the central Apennines (the Pescasseroli, Maiella and Frattura/Scanno faults). They studied time periods with both rapid slip lasting a few millennia with several metres of surface slip, that they interpreted as temporal earthquakes clusters, and periods of relative low slip-rate lasting several millennia with little or no measured surface slip, which they interpreted as temporal earthquake anticlusters. They calculated changes in differential stress and implied strain-rate changes on postulated underlying shear-zones implied by the surface slip recorded by the ^{36}Cl data. Again, they did this using the relationship $\dot{\varepsilon} \propto \sigma^n$ (see Equation (1) for details). They found results consistent with those from Mildon et al. (2022), in that the magnitude of the implied strain-rate and hence slip-rate decreases on fault undergoing anticlusters replicated the slip-rate decreases on receiver faults during anticlusters recorded by the ^{36}Cl data. However, in addition, they showed that strain-rates on shear-zones postulated to exist beneath faults shown to be slipping rapidly in temporal earthquake clusters could be explained by stress increases produced by the downward transfer of stress from a slipping fault. In summary, Roberts et al. (2024) found the same explanation for anticluster formation as that provided by Mildon et al. (2022), and also advanced an explanation for how clusters form. However, the results in both of these papers are limited by the fact that they studied relatively small numbers of faults and thus could not include data on the full picture of fault/shear-zone interaction across the entire width of the extending orogen in the central Apennines.

The approach we have taken to address this limitation is as follows. (1) We present new ^{36}Cl data from 12 faults to augment ^{36}Cl data from 15 faults published in our previous papers (Cowie et al., 2017; Goodall et al., 2021; Mildon et al., 2022; Roberts et al., 2024); together the dataset covers most of the faults within the extending orogen of the central Apennines. (2) We remodel ^{36}Cl data from 6 of the 15 previously published sites because they have not been previously modelled with the code from Beck et al. (2018). (3) We model the ^{36}Cl data from the 12 new sites using the code from Beck et al. (2018). (4) We test whether changes in differential stress implied by the slip-rate changes recovered by modelling of the ^{36}Cl data across the whole extending orogen are of sufficient magnitude to explain overall observations of the characteristic of clustering and anticlustering from the entire ^{36}Cl database.

4. Method

Samples in the database examined have been collected from 27 sites on active normal faults for ^{36}Cl analyses in a field campaign between 2007 and 2015 (see previous paragraph details of the dataset). These ^{36}Cl data, and structural measurements made at the sample sites, are publicly available for study, and can be accessed from a data repositories organised by the UK Natural Environment Research Council (NERC) and British Geological Survey (BGS) (see Acknowledgements and Electronic Supplements 1 and 2), and also in existing papers (Cowie et al., 2017; Goodall et al., 2021; Mildon et al., 2022; Roberts et al., 2024).

Where possible, an attempt was made to sample the faults for ^{36}Cl close to the centres of their map traces, and away from bends in the fault trace (Fig. 3). Sample sites were selected where it could be shown that carbonate fault planes at the surface had been exhumed by earthquake slip, and not affected by local erosion/sedimentation using the criteria developed by Cowie et al. (2017) (Electronic Supplement 1). Locations were selected using these criteria where (1) no erosive channels/gullies or landslide morphologies exist on the footwall or hangingwall of the fault, (2) a clear upper slope and lower slope could be identified across the fault which had been produced during the high erosion rates during the LGM, (3) the contact between the lower slope and fault plane was horizontal ruling out along-strike mass wasting, and (4) where the fault plane was sufficiently preserved to rule out surface dissolution/plucking of the fault plane, evidenced by the preservation of mm-scale frictional wear striae produced by fault slip. The necessity of this approach to exclude erosion and sedimentation contributing to exhumation or burial means that we have not included ^{36}Cl results from other studies in our analysis because our fieldwork shows that those studies did not adhere to the above criteria. The dips of the slopes, fault planes dips, and offsets across the fault scarps were measured in the field (Electronic Supplement ES1).

The fault planes were initially sampled semi-continuously with sample spacings of only 0.12 m (see Cowie et al., 2017), but thereafter sampled discontinuously, with sample spacing up the fault plane of ~30–40 cm. Samples were also excavated from trenches exposing the sub-surface fault planes to help constrain sub-surface production of ^{36}Cl and better constrain the most recent slip. Discontinuous sampling is appropriate because previous studies have shown that denser sampling does not produce improved resolution of the timing and magnitudes of slip-rate fluctuations (e.g. Beck et al., 2018). For example, Mildon et al. (2022) carried out a progressive synthetic degradation of the data for the densely sampled Fiamignano fault in central Italy included in this study. They progressively reduced sample spacings from 0.12 m to 0.5 m, and showed that after 1.3 million iterations of the Beck code (Beck et al., 2018), and convergence between two parallel Markov chains, the results were indistinguishable using from the top 10,000 least squares solutions, and also using the posterior distribution of highest likelihood solutions after 50% burn-in. This is because error bars from accelerator mass spectrometry (AMS) for ^{36}Cl concentrations overlap at sample spacings of less than a few decimetres. Overall, the single least squares solutions differed in detail, but the temporal changes in slip-rate from the full results were indistinguishable. Iezzi et al. (2021) produced similar results through degradation of the densely sampled ^{36}Cl data from Mechernich et al. (2018) for the Pisia fault in Greece. Thus, to extract slip-rate variability, these studies show that discontinuous sampling provide adequate constraints.

The ^{36}Cl samples were prepared using the method detailed in Cowie et al. (2017), including sample inspection for alteration, crushing and sieving, and wet chemistry at the University of Leeds, and underwent AMS for ^{36}Cl concentrations and ICP-OES for elemental concentrations at, and arranged by, SUERC in East Kilbride. Data for the chemistry of the samples is given in Electronic Supplement ES2.

"In this study we modelled the ^{36}Cl data using the Bayesian MCMC reverse-jump code provided by Beck et al. (2018), as described in that paper and summarised in Roberts et al. (2024). The code attempts to replicate the measured ^{36}Cl concentrations through forward modelling in an attempt to retrieve earthquake slip history of that site. The code proposes earthquake histories and calculates the implied ^{36}Cl production and ^{36}Cl preservation within fault plane rock samples for comparison with the measured values. The geometry of the fault scarp and geochemical data for each sample site are input into the code. These data include (a) the dips of the upper and lower slopes, and the dip of the fault plane defined by fieldwork, (2) the offset of the slope in the plane of the fault defined by fieldwork (see ES1 Electronic Supplement 1), (3) the densities of rocks, and the positions of the samples and their ^{36}Cl concentrations and uncertainties as determined through accelerator mass spectrometry, (4) the major and minor element concentrations determination by ICP-OES (see ES2 Electronic Supplement 2), (5) scaling factors for ^{36}Cl production related to the magnetic field and how it varies with elevation and latitude (see ES1 Electronic Supplement 1), and (6) the composition of typical colluvium in the hangingwall of the fault. The code proposes potential earthquake timings drawn from a widely-accepted model of earthquake recurrence (Brownian Passage Time model, BPT), and repeats this millions of times (see ES3 Electronic Supplement 3). The magnitudes and timings of slip events are iterated, as are uncertain parameters such as the density of the colluvium and ^{36}Cl production factors (e.g. production rates and attenuation lengths for spallogenic and muonic ^{36}Cl production), and the timing of ^{36}Cl initial production. The iteration process above is achieved with a Markov Chain Monte Carlo (MCMC) approach, including reverse jumps. The code runs at least 2 parallel Markov chains, and assesses convergence onto a final result using a standard Gelman-Rubin test. The results are presented as a posterior distribution of highest likelihood results (e.g. the median and 90% confidence results after 50% model burn in), and also least-squares solutions, and ensembles of least squares solutions, which represent the best-fits to the ^{36}Cl data (see ES3 Electronic Supplement 3). The code from Beck et al. (2018) focusses on trying to identify changes in slip-rate, rather than the timings or amounts of slip for individual earthquakes".

Once the modelling was complete, we interpreted the resulting slip versus time histories produced after a burn-in period of 50% of the model run, attempting to identify constant or conversely fluctuating slip-rate. The results showed that fluctuating slip-rates are ubiquitous (see ES4 and ES5 Electronic Supplements 4 and 5), so we attempted to constrain durations and magnitudes of slip in high and low slip-rate periods. We did this by identifying inflections in the slip-rate from combinations of (i) the least squares solution for each site, (ii) from inflections in trends represented by ensembles of the top 10,000 least squares solutions for each site, and (iii) from inflections in the 90% confidence bands and median results from the posterior distribution of highest likelihood solutions produced after 50% burn-in. These interpretations of slip-rate inflections are shown in Electronic Supplement ES3, ES4 an ES5, which include the full Bayesian results for each site.

The results from the Mt. Vettore, Leonessa, Laga, Colfiorito (Mt. Le Scalette), Fiamignano and Barete sites have already been modelled using the Beck code (Beck et al., 2018), and published (Mildon et al., 2022) (6 sites). The results from the Pescasseroli, Frattura (Scanno) and Maiella sites have already been modelled with the Beck code and published (Roberts et al., 2024) (3 sites). The remaining 18 sites have not been published with modelling using the Beck code, although the data from 6 of these 18 sites, that is, the Gioia dei Marsi, Parasano, Tre Monti, San Sebastiano, Campo Felice and Roccapretruro sites have been published by Cowie et al. (2017) and Goodall et al. (2021), and modelled using the code presented by Cowie et al. (2017); we re-modelled them using the Beck code for consistency. In summary, in this paper we re-use published data and modelling using the Beck code for 9 sites, but provide more detail on the full modelling results (Electronic Supplement ES3), and present new ^{36}Cl and elemental data from the other sites, and new modelling using the Beck code where this has not previously been conducted. We have not included the results produced by palaeoseismic trenching studies in our analysis of slip-rate variability (e.g. Galadini and Galli, 2000; Cinti et al., 2021), because such studies tend to concentrate on the valuable endeavour of identifying individual palaeoearthquakes, rather than identifying slip-rate variations produced by temporal earthquake clusters, which is the topic of this paper. In fact, it is rare to find time versus slip plots in publications on palaeoseismic trenching, because (a) it is challenging to constrain both the maximum slip per earthquake, given the uncertainty in the relationship between colluvial wedge thickness and coseismic slip, and the timing of individual earthquakes, due to uncertainties in finding dateable material, (b) defining the slip-rate between individual earthquakes of uncertain timing and slip can be challenging, and (c) palaeoseismic records from trenching studies are often either relatively short at just a few millennia, or incomplete due to hiatuses in sedimentation or erosion associated with palaeosols. However a comparison between our ^{36}Cl based results and the valuable results from palaeoseismic trenching could be a fruitful endeavour for future work.

We modelled changes in differential stress that occur when a fault or shear-zone undergoes extensional deformation implied by the ^{36}Cl data, and changes in differential stress implied by the notion that strain in the brittle crust must be compatible within strain in the viscous crust in order to maintain extensional heave with depth (Fig. 2c and d). We modelled the motions implied by the ^{36}Cl as discrete earthquakes rather than creep, because GNSS measurements across the Mt. Vettore fault in the central Apennines showed that metre-scale surface faulting produced by the 30th October Ms 6.6 earthquake occurred in <2 s, and that slip had started before the arrival of strong-shaking at the surface (Wilkinson et al., 2017). The stress modelling used the approach and codes described by Mildon et al. (2022) and Roberts et al. (2024). A summary of this approach is as follows. We modelled the deformation implied by the ^{36}Cl results as discrete earthquakes on the brittle faults, calculating and recording the resulting changes in differential stress on neighbouring receiver faults and receiver shear-zones. For changes in differential stress on receiver shear-zones, we calculated the changes in viscous strain-rate implied by the stress to strain-rate relationship shown in Equation (1). We then use the implied strain-rates to calculate stress transfer onto neighbouring receiver faults and shear-zones produced by shear-zone slip. We use changes in strain-rate on receiver shear-zones to calculate the implied slip-rate on overlying faults by assuming strain compatibility between the brittle and viscous crust (Fig. 2c). Overall, this approach examines feedback cycles between faults and their assumed underlying shear-zones, and between neighbouring fault/shear-zone structures (Fig. 2c and d).

5. Results

Fig. 3 shows the locations of sample sites and the ^{36}Cl concentrations for each sampled fault. It was not possible to sample all the faults in the region because we were unable to identify suitable sites on all faults using the criteria stated by Bubeck et al. (2015) and Cowie et al. (2017). Nonetheless, we think that samples were obtained from most of the faults that are thought to dominate the strain in the region (Faure Walker et al., 2012; Faure Walker et al., 2021; Lavecchia et al., 2022).

Fig. 4 shows the slip histories derived using the Beck et al. (2018) code. Also shown are the expected coseismic *dmax* derived from the fault lengths and the relationships given in Wells and Coppersmith (1994) (see Wesnousky, 2008 for similar relationships). For each site we show the least squares solution which produces ^{36}Cl predictions that are the best fit to the ^{36}Cl data, the ensemble of the top 10,000 least squares solutions, and the highest likelihood solutions from the full posterior distribution of the results after 50% burn-in shown as the 90% confidence bands and the median (typically >500,000 solutions). Detailed modelling results are given in Electronic Supplement 3, and detailed interpretations for each fault are given in Electronic Supplement ES4.

The results demonstrate that temporal fluctuations in slip-rate are ubiquitous across all the sampled sites. The amounts of slip in the periods of relatively high slip-rate are too large to be produced by a single earthquake, given the *dmax* values from scaling relationships between fault length and coseismic *dmax* (Wells and Coppersmith, 1994), implying that several large magnitude surface faulting earthquakes occurred in these time periods, and hence the existence of temporal earthquake clustering. These clusters are separated by time periods where surface faulting earthquakes of the slip magnitudes from Wells and Coppersmith (1994) must have been less frequent or absent, because the amount of recorded slip is smaller than that predicted by that scaling relationship, and in this paper we define these low-slip-rate episodes as anticlusters. The absolute timing of clusters and anticlusters differ between the faults, as do the magnitudes of slip and slip durations for clusters and anticlusters. This is the first time that slip-rate fluctuations alongside clustering and anticlustering have been constrained over a time period as long as 20,000 years for most of the main faults across the entire width of an area of extension.

The magnitudes of the slip-rate fluctuations imply significant changes to the implied earthquake frequency-magnitude distributions and probabilities of earthquake recurrence between different time periods (Fig. 5). For one fault, the Frattura (Scanno) fault, where the slip-rate rate fluctuates between ~5.6 mm/yr in one time period and ~0.1 mm/yr in another, we have calculated the implied annual cumulative rates of earthquakes using the FiSH code from Pace et al. (2016). The implied annual cumulative rates of earthquakes differ by more than an order of magnitude between the two time periods, so implied probabilities of damaging earthquakes in 50 years will differ by a similar amount.

Fig. 6 shows which of the sampled faults, in each 1000-year time period, were experiencing what we interpret to be high slip-rate episodes produced by the temporal clustering of surface earthquakes (this is also shown in an animation, and we recommend this to the reader as it may be easier to visualize the temporal variability; Electronic Supplement 5). We also show two 500 year-long time periods for the most recent millennium. The interpretations of the relatively-high high slip-rate episodes are made using three separate approaches in Fig. 6 and Electronic Supplement 5. These approaches are (a) using only the single least squares solution, (b) using the ensemble of the top 10,000 least squares solutions, and (c) using the 90% confidence bands for highest likelihood solutions from the posterior distribution of results after 50% model burn-in. These three approaches are important to note, because they illustrate that the user has a subjective choice of which approach to use to interpret the timing, amount of slip, and slip duration during clusters and anticlusters. The three approaches also show where a cluster can be identified using more than one approach adding confidence to the overall interpretation.

In each time slice from 15 ka to the present-day, earthquake clusters characterise relatively small numbers of the faults at any given time, with clusters migrating around the overall fault network through time on a millennial timescale (Fig. 6 and the animation in Electronic Supplement 5). At times the activity is concentrated in the centre and parts of the NE flank of the extending region (e.g. the last 500 years and from 14 to 8 kyrs), whilst at other times activity also occurs on the SW flank close to the capital city, Rome (e.g. 6.0–0.5 kyrs). It has previously been reported that faults located across strike from each other have clusters whose timing are out-of-phase between neighbouring faults (e.g. Mildon et al., 2022), whilst in another example activity migrates across strike in two waves from SW to NE between three across strikes faults (Roberts et al., 2024). These patterns are evident within the results shown herein, because they are derived from the same dataset and modelling approach, but in addition cluster migration in other places displays movement between neighbouring faults that exhibit less clear spatial patterns. Nonetheless, we suggest that valuable insights can be gained by compiling the characteristics of the clustering across the entire region as these may help to reveal the causes of the clustering and anticlustering.

Fig. 7 shows a compilation of the data showing the characteristics of clustering across the region (full results and calculations are reported in Electronic Supplement ES4). In the following text we report results mainly for the least squares solution, including results from the highest likelihood results where appropriate, but in Electronic Supplement ES4 we also report the results for the median of the highest likelihood solutions from the full posterior distribution after 50% model burn-in. The results are as follows.

(1) The sampled faults have lengths ranging between 6.3 and 47 km with a mean value of 22.5 km and standard deviation (SD) of 10.9, as reported in the so-called Fault2SHA database reported in Faure Walker et al. (2021) (Fig. 7a). These fault lengths are used

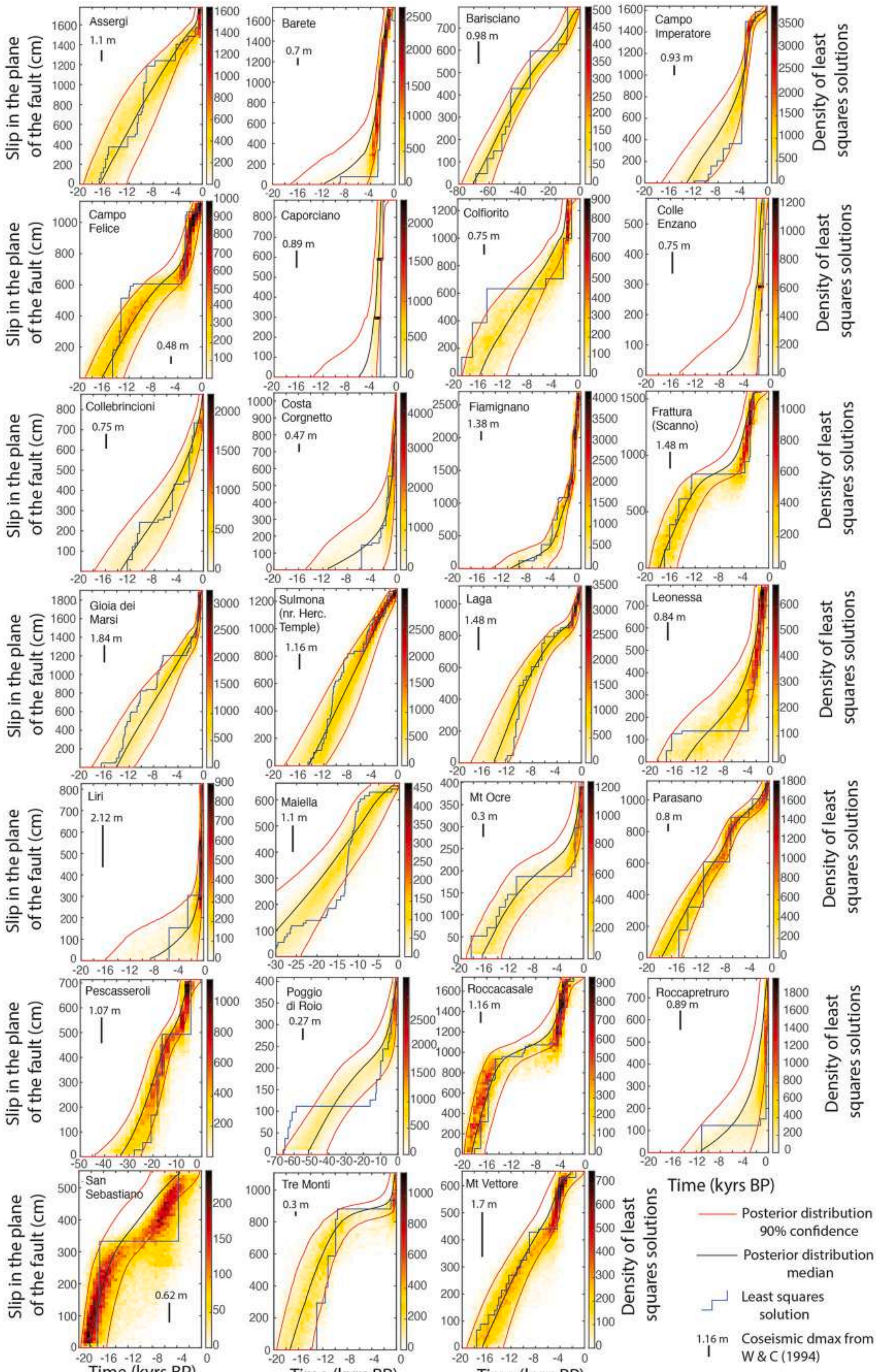

Fig. 4. Slip histories recovered with Beck code from the data in Fig. 3 and Electronic Supplements ES2 and ES3.

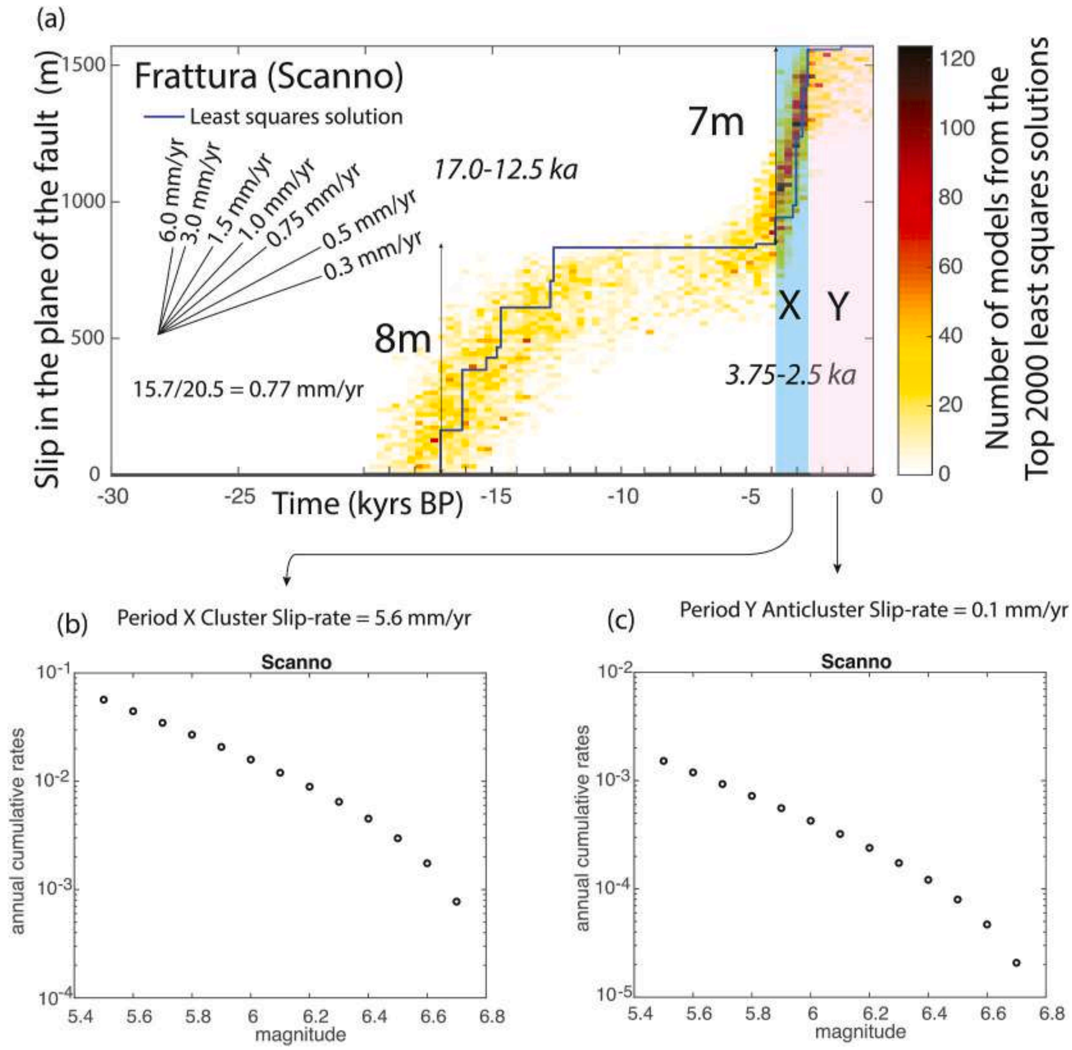

Fig. 5. Earthquake frequency magnitude distributions for two different time periods implied by the slip history derived from the ^{36}Cl data. The annual cumulative rates were calculated by inputting values for the fault length, dip, seismogenic thickness, and slip-rate minimum and maximum into the FiSH code (Pace et al., 2016). The annual cumulative earthquake rates implied by cluster and anticluster slip-rates differ by more than one order of magnitude, emphasising the importance of slip-rate variations for seismic hazard calculations.

to define expected coseismic *dmax* for each of the faults, which have a mean of 0.97 m (see Figs. 4 and 7b).

(2) The faults all dip to the SW, except for the Leonessa fault which dips towards the NE, and have dips in the range of 40° and 71° with a mean value of 56° and a standard deviation of 7.9 (Figs. 3 and 7c).

(3) The long-term slip-rates are defined by the amount of slip over the last ~20,000 years constrained by the modelling results of ^{36}Cl data. These results confirm that for most faults evidence for slip recorded by the scarps is preserved since about 15 ± 3 ka, which previous studies have suggested was the timing of the stabilisation of slopes during the demise of the LGM. The slopes were then offset across the scarps by surface faulting (Piccardi et al., 1999, Roberts and Michetti, 2004; Faure Walker et al., 2012; see Electronic Supplement 1 for slope data, scarp profiles and photos of the fault scarps). For some faults slip has also been preserved from before 15 ± 3 ka (Fig. 4), and this has also been reported and discussed for other bedrock faults scarps in the Mediterranean (e.g. Iezzi et al., 2021; Mechernich et al., 2023 for examples from Greece). As described above, the absence of slip before 15 ± 3 ka for most faults is probably due to (a) relatively high erosion rates during the LGM obscuring surface slip (e.g. see Tucker et al., 2011), but it is important to note that it may also be that (b) some faults may have been in an anticluster at that time. This complicates the choice of a time-period over which to calculate long-term slip-rates. Herein, we have chosen to calculate long-term slip-rates averaged over the last 20,000 years, and these fall in the range of 0.2–1.35 mm/yr with a mean value of 0.57 mm/yr and a standard deviation of 0.26 (Fig. 7d).

(4) In any given 1 kyrs time slice (0.5 kyrs for the last 1000 years), the percentage of the sampled faults experiencing a cluster in both the least squares and the posterior distribution of highest likelihood solutions at 90% confidence is between 7 and 67% with a mean value of 31% and a standard deviation of 17 (Fig. 7e).

(5) There is evidence of clustering in all 2 kyrs time slices if one considers both the least squares solutions and the median solutions from the posterior distributions after 50% burn-in (Fig. 7f and g).

(6) The slip magnitudes in clusters are in the range of 2.5–25 m with a mean value of 5.85 m and a standard deviation of 4.1 for the least squares solutions (Fig. 7h and i). This magnitude of slip is greater than is expected in single earthquakes given the lengths of the faults and the relationships presented by Wells and

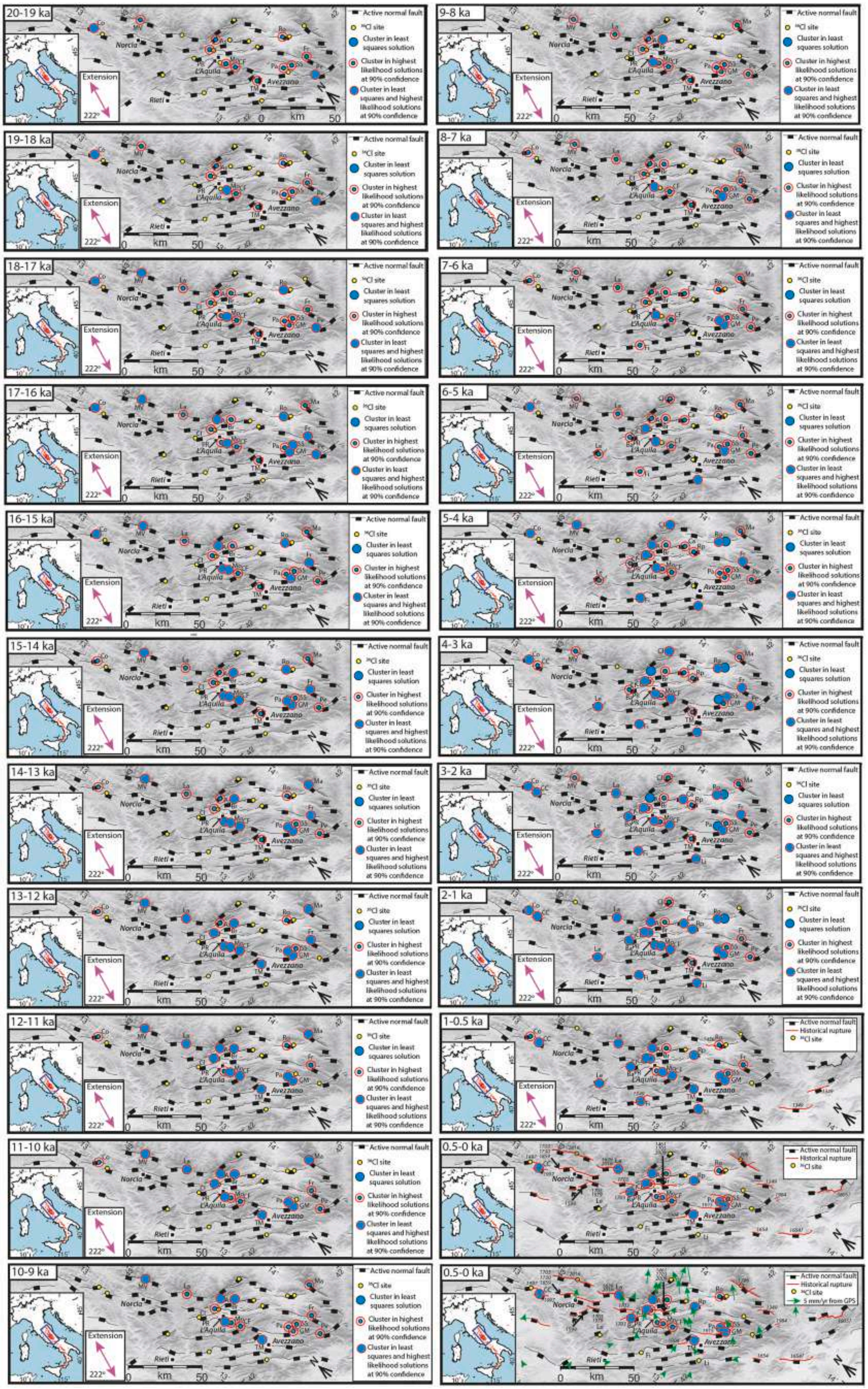

Fig. 6. Maps showing sites experiencing temporal clusters of surface fault earthquakes for different time slices. Time periods are 1000 years, except for 1.0–0.5 ka and 0.5–0.0 ka (500 years). Symbols show whether the cluster is suggested by the only the least squares solution, the highest likelihood solutions at 90% confidence,

or a both the least squares solution and the highest likelihood solutions at 90% confidence. These maps can be visualised as an animation in Electronic Supplement ES5.

Coppersmith (1994) (range of 0.27–2.12 m with a mean of 0.97 and SD of 0.5; Fig. 7b and j). This reinforces the suggestion that the slip in a period of relatively rapid slip cannot be produced by a single earthquake, and so must represent a cluster of surface faulting earthquakes.

(7) The durations of clusters are up to ~9 kyrs, with a mean of 2.83 kyrs and a standard deviation of 1.99 (Fig. 7k), although a higher mean value of 4.26 kyrs is suggested by the median values from the posterior distribution of highest likelihood solutions after 50% model burn-in (Fig. 7i).

(8) The slip-rates in clusters from the least squares solutions fall in the range of 0.24–22.0 mm/yr with a mean value of 3.63 mm/yr and a standard deviation of 4.2 (Fig. 7m), with a mean value of 1.42 mm/yr suggested by the median values from the posterior distribution of highest likelihood solutions after 50% model burn-in (Fig. 7n). The slip-rate values from the least squares solutions imply slip-rate enhancement values (slip-rate in the cluster divided by the long-term slip-rate over 20 kyrs, SRE) in the range of 1.21–30.86 with a mean of 6.24 and a standard deviation of 7 (Fig. 7o and p). Note that the very high slip-rates within the distribution of up to 22 mm/yr from the least squares results (e.g Fig. 7m) may be overestimates produced by a combination of the limited resolution of timing recorded by the ^{36}Cl data and the limited ability of the modelling code to resolve the timing of individual earthquakes within very short duration clusters. However, we suggest the achieved time resolution is the state-of-the-art at present, so the exact duration of very short-lived clusters and hence the exact SRE values require future study.

(9) The slip-rates in clusters exceed those averaged over 20 kyrs (Fig. 7q).

(10) Anticlusters are best constrained where we have been able to measure both their start and end times, that is, where they have been shown to occur in time between two clusters. Results for such anticlusters have durations that fall in the range of 1.9–12.7 kyrs with a mean value of 7.09 kyrs and a standard deviation of 3.3 (Fig. 7r and s). The median anticluster durations for the faults close to the SW flank of the Apennines (the Fiamignano, Leonessa and Liri faults), although less well constrained due to the absence of measured start times for the anticlusters, have a mean value for anticluster duration of at least 15.33 ± 1.23 kyrs, much longer than the anticluster durations recorded for faults on the NE flank of 6.2 ± 3.53 kyrs (Fig. 7t).

(11) The slip-rates in the anticlusters are lower than those within clusters, with a value as low as zero mm/yr from the least squares solutions for the anticlusters, or a mean of 0.51 mm/yr from the values obtained for the median of the posterior distribution of highest likelihood solutions (Fig. 7u). For comparison we note a mean for the clusters of 3.41 mm/yr from the least squares solutions, or a mean of 1.42 mm/yr from the median values from the posterior distribution of highest likelihood solutions after 50% burn-in (compare Fig. 7m, n and 7u). However, we suggest that the slip-rates in anticlusters are challenging to quantify. This is because although they can appear as low as zero from the least squares solutions, the smallest surface slip size we allowed whilst using the code from Beck et al. (2018) was 10 cm, so zero slip-rate values may be underestimates. Also, the results from the median slip histories from the posterior distribution of highest likelihood solutions after 50% model burn-in may be overestimates because they include solutions that will fit the measured ^{36}Cl data less well than the least squares solution. Nonetheless, the time versus slip histories in Fig. 4 show that the trajectories for slip have lower slopes in the times between clusters than (a) the slip-rates averaged since 20 ka, defined by the total slip and the timing of slip preservation defined by the ^{36}Cl data, and (b) the slip-rates within clusters.

Overall, the results confirm that the study of ^{36}Cl from fault planes provides the opportunity to constrain the slip-rate histories of multiple faults across the whole width of an extending orogen, with a continuous time sample, lacking hiatuses, over a time period, in this example, of ~20 kyrs. They also allow characterisation of the slip-rate variability, clustering and anticlustering (Fig. 7). However, note that the disadvantages of the ^{36}Cl approach are as follows. (i) The slip-histories are retrieved from the ^{36}Cl data using modelling, in this case using the code from Beck et al. (2018), yet other codes exist (Schlagenhauf et al., 2010; Cowie et al., 2017; Tikhomirov et al., 2019; Tesson and Benedetti, 2019), each with their own advantages and disadvantages. The reasons for using the Beck et al. (2018) code explained briefly above, and in detail in Roberts et al. (2024), but to summarise, we feel it is best suited to studying slip-rate histories. (ii) Although the least squares solutions reveal the best fit to the ^{36}Cl data, and document the timing and magnitudes of slip for individual model earthquakes, there are thousands of other solutions that fit the ^{36}Cl almost as well, and these will have slightly different timings for the model slip events, and also different slip magnitudes. This is why it is important to consider results represented by the ensembles of the top 10,000 least squares solutions, and the 90% confidence and median solutions from the posterior distribution of highest likelihood solutions. As mentioned above, this introduces uncertainty into how one should interpret the data, so we have considered all three visualisations of the results, and concentrate on studying slip-rate variability rather than identifying individual earthquakes.

6. Discussion

The results show that deformation associated with active normal faults in the central Apennines is characterised by fluctuating slip-rates on individual faults on a millennial timescale, and this has been facilitated by interpretation of ^{36}Cl data. Slip on individual faults during time periods when they experience relatively high slip-rates can be several metres or more, and hence too large to be explained by the occurrence of single earthquakes, implying the occurrence of temporal clusters of surface faulting earthquakes. Although the regional extension-rate over the last few decades has been measured to be ~3–4 mm/yr using GPS (Figs. 6 and 8; D'Agostino et al., 2011), and more recently with InSAR (Daout et al., 2023), slip-rates within temporal earthquake clusters on individual faults can accommodate or exceed this value for periods of time lasting a few thousand years whilst other faults enter periods of quiescence. Only a relatively small percentage of the faults are experiencing high-slip rates in any 1000-year time-period, and the geographic positions of the faults experiencing high slip-rate episodes change through time.

These results are of interest in a general sense because we suggest they represent the first time that data characterising slip-rate variability and the temporal clustering of surface faulting earthquakes have been compiled from across an entire extensional fault system on a timescale as long as 20 kyrs. However, more specifically, these results have important implications for assessing the seismic hazard in the region because they imply fluctuations in the rate of seismicity on individual faults (Fig. 5) and changes in the locations of seismicity through time (Figs. 6–8; Electronic Supplement 5). They also allow us to study the mechanics of extension because they allow assessment of the likely mechanisms responsible for causing the fluctuations in fault activity. Below we discuss various aspects of our results in turn.

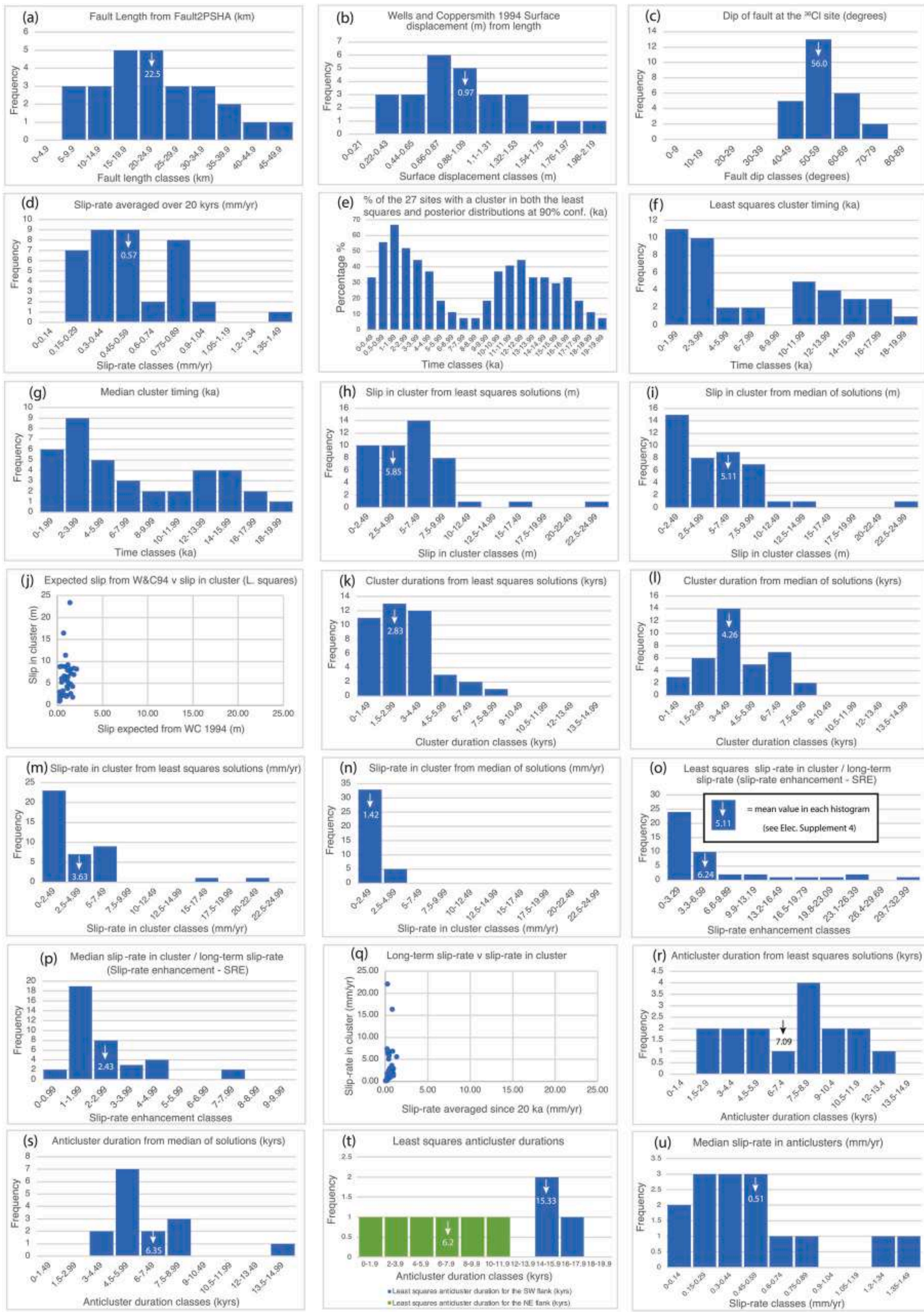

Fig. 7. Characteristics of Clustering in central Italy from slip-histories derived from ^{36}Cl data. Histograms and graphs showing the distributions within our dataset of (a) fault lengths, (b) expected coseismic *dmax* from Wells and Coppersmith (1994), (c) fault dips, (d) long-term slip-rate over 20 kyrs, (e) percentage of faults showing a cluster in each 1000 year time slice, (f) and (g) cluster timings, (h) and (i) slip in clusters, (j) expected coseismic *dmax* from Wells and Coppersmith (1994) compared to slip in clusters, (k) and (l) cluster durations, (m) and (n) slip-rates in clusters, (o) and (p) slip-rate in clusters divided by the long-term slip-rates (Slip Rate Enhancement; SRE), (q) Long-term slip-rate versus slip-rate in cluster, (r) and (s) anticluster durations, (t) comparison of anticluster durations between the SW and NE flanks of the Apennines, (u) slip-rate in anticlusters. White arrows with numbers indicate the mean values.

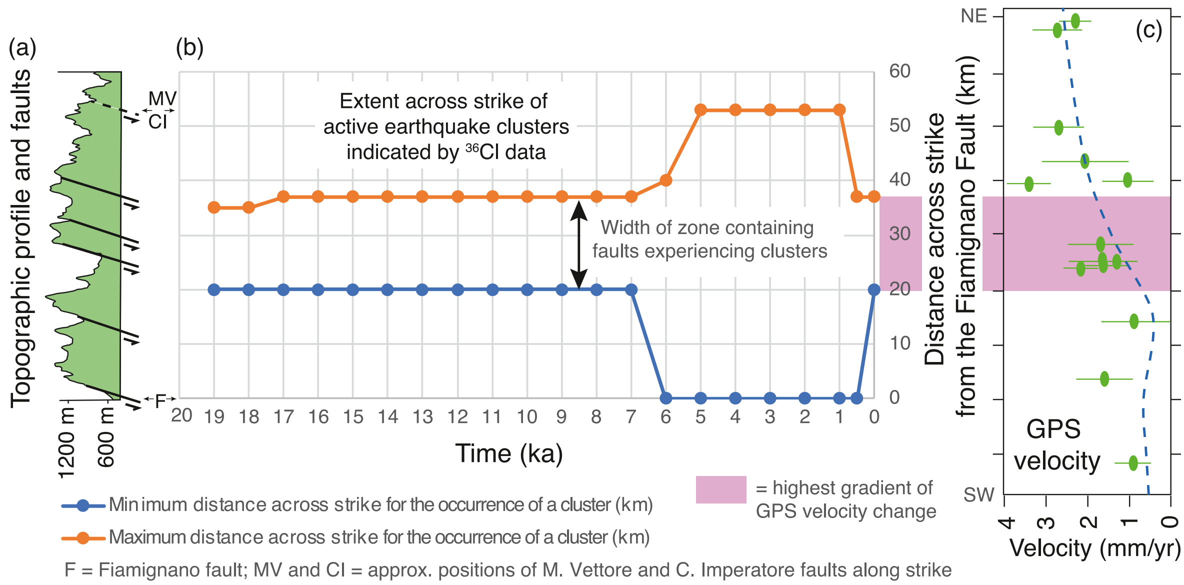

Fig. 8. Distance across strike within which clustering occurs. Distance across strike was measured from the Fiamignano fault along the azimuth N057°, by projecting sites perpendicular to this azimuth. The topographic profile in (a) was derived from SRTM data and the transect is located in Fig. 3. GPS velocities are from D'Agostino et al. (2011). Clustering was confined to a relative narrow zone from 20 to 7 ka, a wider zone from 7 to 0.5 ka, and has been confined to a relative narrow zone from 0.5 ka to present. The highest gradients in velocity defined by GPS coincide with the relatively narrow zone of clustering that has existed since 0.5 to the present-day.

6.1. Implications for interpreting results from in situ ^{36}Cl cosmogenic dating of fault scarps

Before we discuss tectonics, we cannot ignore the fact that debate exists in the literature, and within the earthquake science community, about the best approach for interpreting the results of sampling fault planes for ^{36}Cl, and even whether such results can be used to assess slip through time produced by earthquakes. In this section we discuss various aspects of this debate, including (i) the role of surface erosion, sedimentation and mass wasting, and (ii) interpreting the timing of individual earthquakes versus concentrating on slip-rate variations over time periods that may contain multiple earthquakes. We argue that results from ^{36}Cl can be used to assess slip produced by earthquakes and how slip-rates fluctuate through time.

It has been suggested that erosion and sedimentation may contribute to the exhumation of the fault planes (Kastelic et al., 2017), and that this may be concentrated at so called pluvial periods with high erosion and exhumation rates accompanied by activation of landslides and mass wasting in the European Alps (e.g. Zerathe et al., 2014). However, in this study we emphasise that all the sample sites have been chosen specifically to exclude the possibility of erosion, mass wasting and sedimentation. We have done this by avoiding locations close to hangingwall and footwall gullies, landslide morphology, and where the hangingwall to fault plane contact is not horizontal and along-strike mass movement may have occurred. In other words, it is the favourable geomorphological settings of our sample sites that have allowed us to interpret the results in terms of tectonic slip produced by earthquakes. Our claim that our choice of sample sites excludes non-tectonic processes as dominating the exhumation is consistent with the observation that we do not see rapid exhumation concentrated at times known to have high rates of landscape evolution (Fig. 7f and g). For example, there is no concentration of clusters at 4.2 kyrs, the time of a well-known pluvial period in the European Alps (e.g. Zerathe et al., 2014). Therefore, we suggest that the periods of rapid exhumation we have measured with ^{36}Cl are produced by temporal clusters of surface faulting earthquakes and not erosional mass-wasting episodes driven by climatic processes. Moreover, Roberts et al. (2024) have shown that erosion rates recorded over a few years close to published fault-plane ^{36}Cl study sites by Kastelic et al. (2017), which these latter authors suggest are responsible for the exhumation, cannot apply to the long-term, millennial timescale exhumation. This is because the erosion rates reported by Kastelic et al. (2017) imply ^{36}Cl concentrations that, for the example of the Fiamignano fault, are 7.02 ± 2.32 times lower than the measured ^{36}Cl values, and so do not explain the longer-term exhumation over the last 15–20 kyrs. Thus, (a) our choice of sample sites, (b) the lack of rapid exhumation measured at known times of rapid surface erosion during pluvial periods, and (c) the fact that measured erosion rates over a few years cannot apply to the longer term, add to our confidence that exhumation via tectonic fault slip since the demise of the LGM is the dominant signal in our ^{36}Cl dataset.

There is ongoing debate about whether ^{36}Cl data from fault planes should be interpreted in terms of the timing of individual earthquakes, versus concentrating on slip-rate variations over time periods that may contain multiple earthquakes. We note that some research groups have concentrated on the former (e.g. Benedetti et al., 2002, 2003, 2013; Palumbo et al., 2004; Schlagenhauf et al., 2010, 2011; Mozafari et al., 2019; Tesson and Benedetti, 2019) and others on the latter (Cowie et al., 2017; Iezzi et al., 2021; Mildon et al., 2022; Roberts et al., 2024). Here we explain in more detail why we concentrate on the latter approach. Firstly, we have concerns about whether individual earthquakes can be resolved within ^{36}Cl datasets, for example by attempting to recognise "cusps" on plots of the ^{36}Cl concentration versus height on the fault plane (e.g. Benedetti et al., 2002, 2003; Palumbo et al., 2004; Schlagenhauf et al., 2010, 2011; Mozafari et al., 2019; Tesson and Benedetti, 2019). We have concerns because for densely sampled ^{36}Cl datasets such as that for the Fiamignano fault (Fig. 3; Electronic Supplements 2 and 3), ^{36}Cl concentrations show variations that appear to be non-systematic over increments of only 10 cm difference in position on the fault planes, in many cases with overlapping error bars, so cusps are not obvious through visual inspection. Secondly, it is important to remember that the ^{36}Cl concentration produced by an exposure history is influenced by the calcium concentration in each individual sample, because spallation of calcium atoms is one of the main production pathways for ^{36}Cl (Gosse and Phillips, 2001). In other words, higher numbers of calcium targets for spallation within a sample means greater ^{36}Cl production from this production pathway, and hence higher ^{36}Cl concentrations within that sample. Therefore, one cannot simply assess variations in ^{36}Cl concentration up a fault plane in terms of cusps, via for example probability density functions, as solely due to a tectonic origin, as they may be influenced by variations in calcium concentration. Thirdly, with our current abilities to limit the sizes of uncertainties associated with sample chemistry and AMS, and our current abilities to model the data, studying fault planes with very high densities of samples may not reveal extra information about the slip history. As mentioned above, Mildon et al. (2022) and Iezzi et al. (2021) artificially degraded densely sampled ^{36}Cl datasets for the Fiamignano fault in central Italy and the Pisia fault in central Greece respectively. They showed that no extra information on tectonic slip emerges when decreasing the sample spacing on the fault plane from ~40 to 50 cm sample spacing to as low as ~12 cm. In detail, 12 cm or 40–50 cm sample spacings provide very similar slip histories implied by the ensembles of the top 10,000 least squares slip versus time histories, and the median and 90% confidence intervals from the posterior distribution of hundreds of thousands of highest likelihood slip history solutions after 50% burn in. The single least squares solutions may well differ between 12 cm or 40–50 cm sample spacings, but the details of these single solutions should not be over emphasised because many other similar solutions exist which fit the data almost as well within uncertainty. Therefore, it is vital to consider the distribution of slip histories within the ensembles of results described above, and the ensemble results for 12 cm or 40–50 cm sample spacings are essentially indistinguishable. This confirms that at present, very high densities of samples may not reveal extra information about the slip history.

In summary, despite the debate about the utility of ^{36}Cl studies in earthquake science, in this study we attempt to recognise periods of high or low slip-rate containing multiple earthquakes from ensembles of results, rather than solely the least squares solution, or trying to recognise individual earthquakes. We suggest that this approach to interpretation can advance our knowledge of earthquake recurrence because it facilitates testing of hypotheses for mechanistic cause(s) of slip-rate variability and temporal earthquake clustering, and we discuss this below.

6.2. Implications for deformation across entire networks of normal faults

Our results agree with Benedetti et al. (2013) in that strain accumulation on individual faults occurs during relatively short time periods marked by temporal clusters of surface faulting earthquakes. However, we do not find evidence for the occurrence across the whole fault system of the three time periods that they interpret to represent high activity rates during so-called "supercycles" of clustered earthquakes (1.5 ± 1 ka; 4.5 ± 1 ka and 11 ± 1 ka; see their Fig. 6), separated by times of relative quiescence. For example, we find high activity rates between 2-4 ka and 12–20 ka at times when their results suggest relative quiescence (Fig. 7f and g). This may be because they sampled a relatively small percentage of the faults in the region. It may also be because the absolute timing of their proposed slip periods is influenced by their use of "pre-exposure" in their attempt to constrain early ^{36}Cl production. They use a wide range of pre-exposure values of 0.6 kyrs, 2.7 kyrs, 3.0 kyrs, 1.5 kyrs, 28 kyrs, 5 kyrs and between 2.5 and 13.0 ka for the seven faults they study. The values chosen for pre-exposure influence the interpretations of the absolute timings of slip events because such values dictate how much of the total ^{36}Cl concentration in a sample is produced early in the exhumation history at depth, prior to exposure of the samples to ^{36}Cl production close to or at the surface, which in turn influences the amount of ^{36}Cl remaining to constrain the ages of slip events. In contrast, we use the Beck et al. (2018) code which does not require the input of a value for "pre-exposure", but instead draws potential slip histories from a Brownian Passage Time model of earthquake recurrence to investigate the slip, including slip that influenced early ^{36}Cl production at depth (see Beck et al., 2018; Roberts et al., 2024 for details of how this is accomplished). We could re-model the ^{36}Cl data from Benedetti et al. (2013) using the Beck code, but we prefer not to do this because their dataset was collected and published prior to the publications of Bubeck et al. (2015) and Cowie et al. (2017), and hence does not adhere to the sampling criteria suggested by these authors to exclude erosion and sedimentation and mass wasting, and our own fieldwork confirms that such surface processes have affected those sites. Thus, although we agree with the valuable and pioneering work of Benedetti et al. (2013) about the existence of activity clustered in time, we prefer our interpretations of the distribution in time of the clusters shown in Fig. 7f and g.

We also emphasise that, in addition to the timing of clusters, the spatial changes in positions of clusters through time provide important insights into the tectonics (Figs. 6 and 8; Electronic Supplement 5). Some time periods exhibit clustering along a relatively localised zone in the central part of the relatively high topography of the Apennines, without activity on the SW and NE topographic flanks of the Apennines (e.g. time periods 19–7.0 ka and 0.5 ka to present). This is reminiscent, at least in terms of geometry, of zones of localised extensional deformation caused, for example, by evolving crustal thermal structure and rheology that developed over millions of years, such as in the late-Jurassic of the North Sea or the Gulf of Corinth, Greece (Cowie and Roberts, 2001; Cowie et al., 2005). Other time periods exhibit clustering that is spread across the whole width of the Apennines extensional orogen (e.g. 5.0–1.0 ka; Fig. 8). This is reminiscent, at least in terms of geometry, of orogen-wide extension interpreted via deformation of a continuum, for example, the Quaternary deformation in Tibet (England and Molnar, 1997). Thus, the results herein reveal that both localised and orogen-wide deformation exist in the same location separated in time by only a few millennia. This suggests that exploring the rheology of the deformation using only a localised model, or alternatively using only a distributed model, may not reveal important aspects of the deformation that occur on a millennial timescale. In fact, for the central Apennines, the position of clusters across strike defined by ^{36}Cl for the last 500 years matches the location where geodetic data from GPS and InSAR suggest that there is an increased gradient in velocity due to extensional faulting (D'Agostino et al., 2011; Daout et al., 2023) (Fig. 8). It is encouraging that GPS, InSAR and ^{36}Cl data agree in this regard. However, before 500 years ago, when three > Mw 6.0 earthquakes occurred on the 9th September 1349 AD, of which two were certainly on the SW flank of the Apennines (Galli and Naso, 2009; Cowie et al., 2017; Galadini et al., 2018), results in this paper confirm that high fault activity rates were more widely spread across the entire width of the deforming extensional orogen (Electronic Supplement 5; Figs. 6 and 8). We will never know if geodetic rates would have recorded more widespread extension across strike before 500 years ago, but one interpretation of their agreement after this time suggests that geodesy may well have recorded more widespread extension before 500 years ago. Overall, fluctuations in the width of the deforming zone on a millennial timescale have important implications for seismic hazard and the implied mechanics of the deformation as discussed below. However, first we investigate the process(es) that are responsible for the slip-rate variability and temporal earthquake clustering.

6.3. Implications for the causes of temporal earthquake clustering

Above we stated that the results in this paper provide a dataset that can be used to test hypotheses suggested to explain earthquake clustering, such as (i) least work arguments if slip in a cluster is limited by dynamic topography (Cowie et al., 2017), (ii) strength variations in underlying shear-zones due to annealing and/or fluid interactions (e.g. Dolan et al., 2007, 2016), (iii) stress interactions between neighbouring fault/shear-zone structures (Mildon et al., 2022; Roberts et al., 2024), or (iv) rate and state friction (Biemiller and Lavier, 2017).

In terms of testing hypothesis (i), that is, least work arguments, Mildon et al. (2022) showed that synchronous clusters can occur on both the NE and SW flanks of the Apennines, and our results reinforce this finding (e.g. the time period between ~5.0 and 0.5 ka shown in Fig. 8). This observation is contrary to the model suggested by Cowie et al.

(2017) whereby clusters on one flank are accompanied by flexural restoring forces that increase the rate of work, so to minimize energy dissipation in the system as a whole, the locus of fault activity shifts to the faults on the opposite flank. Thus, the observations do not match model the prediction from Cowie et al. (2017), so, following Mildon et al. (2022), we discount least work arguments as the dominant cause of clustering in the Apennines.

In terms of testing hypothesis (ii), that is, strength variations in underlying shear-zones due to annealing and/or fluids, a direct model test would require access to samples from within an actively-deforming viscous shear-zone beneath a fault undergoing the transition from an anticluster to a cluster, to enable measurements of the nature and rates of microstructural change and fluid flux, and this is not currently possible. An indirect test may be possible in an experimental rock deformation laboratory, but even with this it is challenging to quantify microstructural evolution within a sample during the experimental run, and the experiment would need to be scaled correctly to simulate the strain-rates during the transition from an anticluster to a cluster. Thus, a hypothesis test for (ii) is challenging.

In terms of testing hypothesis (iv), that is, the effects of rate and state friction, similar problems exist in that a direct model test would require access to samples from within an actively-deforming frictional gouge-zone along a fault undergoing the transition from an anticluster to a cluster, to enable measurements of frictional properties, and again this is not currently possible. Again, an indirect test may be possible in an experimental rock deformation laboratory, but even with this it is challenging to quantify microstructural evolution within a sample during the experimental run, and again the strain-rates would need to be scaled correctly to simulate the transition from an anticluster to a cluster. In other words, it is challenging to directly test the applicability of hypotheses (ii) and (iv) because of the challenges of accessing actively-deforming samples to make measurements to compare with the documented clustering characteristics (Fig. 7).

However, for (iii) stress interactions between neighbouring fault/shear-zone structures, although we cannot measure stresses directly from within an active shear-zone, we can conduct an indirect hypothesis test by modelling stress transfer because the dominant factor controlling this variable is the geometry of the interacting fault system, with relative stress changes varying with distance, azimuth and depth (Figs. 1, 2, 9 and 10). To test hypothesis (iii), we compare measured slip-rate enhancement implied by the ^{36}Cl data with that predicted by stress modelling combined with a widely used quartz flow law for continental crust from Hirth et al. (2001). We note that the mean value for measured slip-rate enhancement (SRE) in clusters for the least squares solutions from the ^{36}Cl data is 6.24, and from the median slip history solutions is 2.43 (Fig. 7o and p, and Fig. 9). Using the flow-law for dislocation creep in quartz from Hirth et al. (2001), and values to use in this flow-law given by Mildon et al. (2022) plus their approach, values of 2.43–6.24 for slip-rate enhancement can be produced by 3.13–7.53 MPa increase in differential stress within a viscous shear-zone deforming at depths of 15–16 km (Fig. 9; calculations shown in Electronic Supplement ES6). Values of 3.13–7.53 MPa increase in differential stress on a shear-zone beneath the viscous-brittle transition are within the range expected at 15–16 km given an earthquake with 1 m of slip on typical normal fault/shear-zone like those we study, e.g. the Pescasseroli fault (Fig. 9d). Thus, the predicted values would produce slip-rate enhancement factors (SRE) large enough to match the values of 2.43–6.24 implied by the ^{36}Cl data. In other words, we suggest that a single earthquake rupture on a

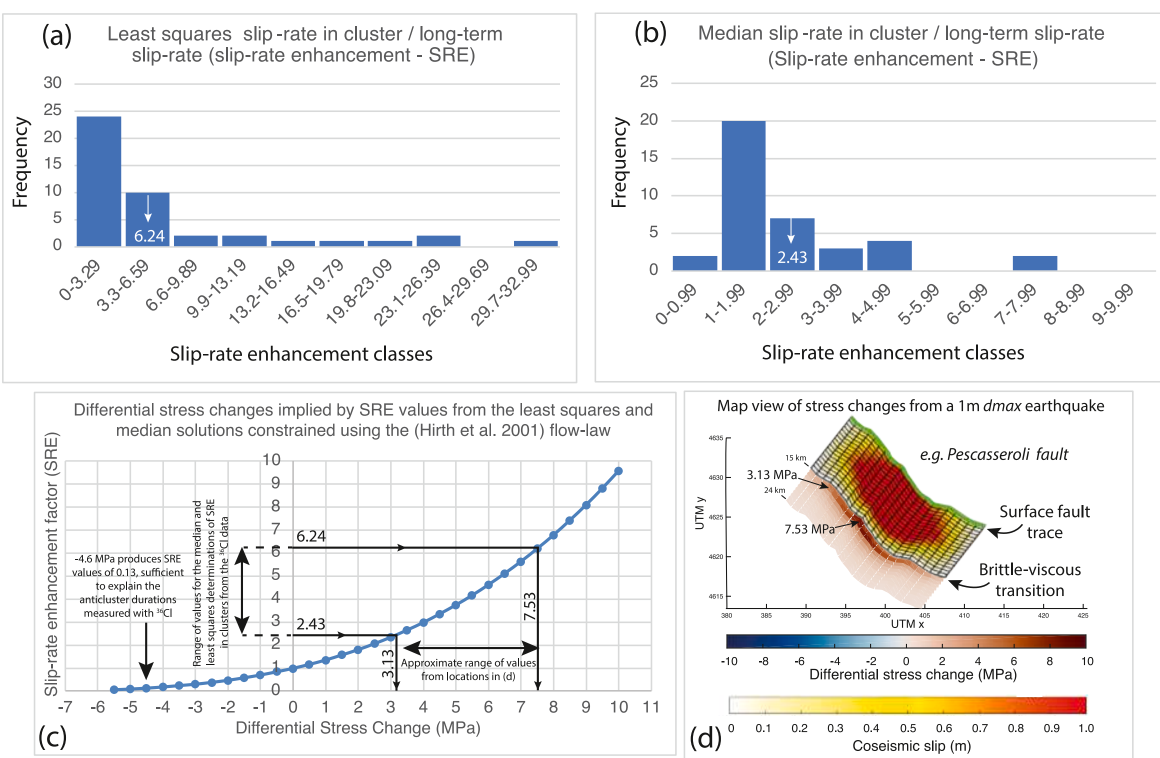

Fig. 9. Stress change and slip-rate enhancement (SRE). (a) Histogram of slip-rate enhancement values calculated from the slip-rate in clusters from the least squares solution divided by the long-term slip-rate over 20 kyrs (b) Histogram of slip-rate enhancement values calculated from the slip-rate in clusters, from the median slip-rate from the posterior distribution of highest-likelihood solutions, divided by the long-term slip-rate over 20 kyrs. White arrows with numbers indicate the mean values. (c) Differential stress changes needed to produce the mean SRE values calculated in (a) and (b) using the flow law dislocation in quartz from Hirth et al. (2001) (see Mildon et al., 2022 for the flow law calculator used herein). (d) Changes in differential stress at 15.5 km depth within a shear-zone beneath, and with the same dip, as the overlying fault which has experienced a 1 m *dmax* earthquake with 40% of the slip at depth making it to the surface (e.g. the Pescasseroli fault located in Fig. 3). Overall, this figure shows that values for differential stress change needed to produce the slip-rate enhancements implied by the ^{36}Cl data are similar to those produced by a surface faulting earthquake in central Italy.

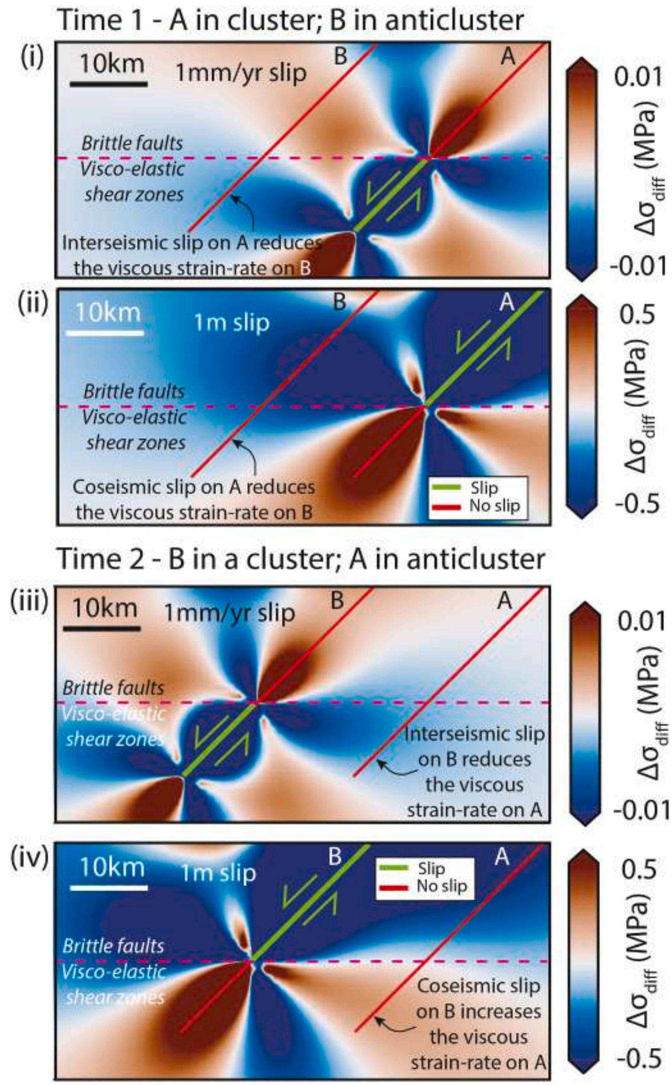

Fig. 10. Proposed explanation for clustering and anticlustering. (i) Time 1 - Slip on shear-zone A loads its overlying fault, and vice versa (ii). This positive feedback on fault/shear-zone A produces a period of rapid slip-rate containing large magnitude surface faulting earthquakes. Stress on shear-zone B is reduced by coseismic slip and interseismic shear-zone slip on A (i and ii), and the reduction becomes more intense during repeated rupture and shear-zone slip on A. This reduction in differential stress reduces the strain-rate associated with shear-zone B. However, the differential stress on shear-zone B is not zero and is being increased by regional tectonics and topographic loading, so although it slips at a reduced rate, eventually it will load fault B enough for it to rupture. The period of rapid slip on A ends and rapid slip will transfer to B. (iii) Time 2 - Slip on shear-zone B loads its overlying fault and vice versa (iv). This positive feedback on fault/shear-zone B produces a period of rapid slip-rate containing large magnitude surface faulting earthquakes. Coseismic slip and interseismic slip on B have opposite effects in terms of stress changes on shear-zone A, with the former increasing the differential stress and the latter decreasing the differential stress. The differential stress on shear-zone A is not zero and is being increased by regional tectonics and topographic loading, so although it slips at a reduced rate, eventually it loads fault A enough for it to rupture. This causes the situation to revert back to that shown in Time 1. The durations of clusters and anticlusters will be determined by the interactions between the two structures which will be controlled by aspects of the fault geometries such as the fault spacing, and fault dip directions. For example, differential stress on shear-zone B, which is located in the dip direction of A, is reduced by both coseismic slip on Fault A and interseismic slip on shear-zone A (see i and ii). In contrast, differential stress on shear-zone A, which is located in the opposite direction to the dip direction of B, is increased by coseismic slip on Fault B, but reduced by interseismic slip on shear-zone B (see iii and iv). Thus, over time, shear-zone B experiences more intense stress reduction than shear-zone A, and hence a greater reduction in strain-rate, and this will produce longer anticlusters on shear-zone B. This implication of the proposed model is consistent with the observation that anticluster duration is relatively long on the SW flank of the Apennines compared to the average for the whole system of sampled faults which predominantly dip to the SW (compare Fig. 7i and u).

brittle fault transfers a positive differential stress change down to the underlying shear-zone (see also Ellis and Stöckhert, 2004), with a magnitude large enough to increase the strain-rate to extent that is consistent with the measured slip-rate fluctuations implied by the ^{36}Cl data. We suggest that this could be the mechanism that initiates an earthquake cluster. Although the strain-rate on a shear-zone will decrease in the post-seismic phase, the increased strain-rate on the shear-zone after the overlying earthquake will in turn increase the stress on the overlying fault (Fig. 2d), leading to positive feedback loop and repeated re-rupture of the overlying fault, and hence repeated differential stress increases and strain-rate increases on the underlying viscous shear-zone. Indeed, this must occur to maintain strain compatibility between brittle faults and their underlying shear-zones (Cowie et al., 2013; see inset in Fig. 2c). By strain-compatibility, we mean that the horizontal extension accommodated by a shear-zone, over a time period containing multiple surface faulting earthquakes, must match the horizontal extension accommodated by the overlying brittle fault (Fig. 2c). This time-period includes multiple coseismic, postseismic and interseismic episodes, and the ^{36}Cl data record the summed strain from all these episodes. So, even though the raised differential stress and hence viscous strain-rates will decay in the postseismic period, the total strain in the viscous shear-zone during a cluster will match that across the brittle fault recorded by the ^{36}Cl data (e.g. see simulations of this by Shimamoto and Noda, 2014; Allison and Dunham, 2018). In summary, over a time-period containing numerous earthquakes and intervening postseismic and interseismic deformation, the predicted increase in slip-rate on the brittle fault, that is, the SRE, would match the SRE predicted for the underlying viscous shear-zone, given the modelled changes in differential stress on the underlying shear-zone and the dislocation creep flow law. Overall, we suggest that the initiation of a cluster and its continuation through time are caused by earthquakes increasing the differential stress on their underlying shear-zones followed by positive feedback between shear-zone slip, upwards stress transfer, earthquake slip and downwards stress transfer.

To further test hypothesis (iii), we now discuss what may control the nature of anticlusters. The duration of anticlusters across all the ^{36}Cl sites we study has a mean value of 7.09 kyrs, but we note that lower values of 6.2 kyrs exist for the NE flank of the Apennines, with higher values of 15.33 kyrs for the SW flank (Fig. 7r and t). We suggest that this difference is produced because there is a structural control on anticluster duration produced by the fact that most faults in the region dip towards the SW (Fig. 3), and stress transfer across strike for dipping normal faults is asymmetric (Fig. 10). For the fault/shear-zone spacings in Fig. 10, shear-zones in the hangingwall relative to slipping fault/shear-zone structures receive stress decreases from both coseismic slip on brittle faults and interseismic slip from viscous shear-zones (Time 1 in Fig. 10). In contrast, shear-zones in the footwall locations relative to slipping fault/shear-zone structures receive stress increases from coseismic slip on brittle faults across strike, but stress decreases from interseismic slip on viscous shear-zones across strike (Time 2 in Fig. 10). Thus, because of the predominant dip of faults to the SW in the Apennines, cumulative stress decreases will tend to be larger in hangingwall locations like the SW flank of the Apennines. To test whether stress transfer associated with this asymmetry can produce slip-rate changes of sufficient magnitude to match those from the ^{36}Cl results, we calculate the changes in earthquake recurrence intervals on the SW flank for times when clustering is localised ~12–25 km to the NE in the high topography of the Apennines, for example between 20-7 ka and 0.5 ka to the present-day (Fig. 8). The mean long-term slip-rate averaged since 20 ka from the entire ^{36}Cl dataset is 0.57 mm/yr (Fig. 7d), and assuming a mean coseismic *dmax* of 0.97 m (Fig. 7b), this implies a recurrence interval of 1701 years for such earthquakes. For the SW flank, an increase of a recurrence interval to about 15 millennia from about 2 millennia represents a slip-rate enhancement factor of 0.13, and this can be produced by a stress reduction on the SW flank shear-zones of −4.6 MPa (Fig. 9; Electronic Supplement 6). A stress reduction of −4.6 MPa at 15.5 km depth on a shear-zone in a hangingwall location is achieved after 11 m slip on a fault/shear-zone structure located 12.5 km into its footwall (Fig. 1b). The ^{36}Cl data show that slip magnitudes in each cluster from the least squares solutions are in the range of 2.5–25 m, so 11 m of slip in a cluster is not implausible (Fig. 7h). Therefore, it is plausible that clusters of 11 1-m earthquake slip events with intervening interseismic slip on underlying viscous shear-zones occurred in the centre of high topography of the Apennines and produced the anticlusters lasting 15 millennia on the SW flank. We suggest that this could be the mechanism that produces longer anticluster durations for faults on the SW flank of the Apennines close to Rome, and the initiation and continuation of anticlusters in general, and hence the observations are consistent with the hypothesis in Fig. 10. Overall, reductions in differential stress on viscous shear-zones underlying brittle normal faults produced by deformation across strike appears to be a plausible explanation for the formation of anticlusters, with anticlusters terminating when their underlying shear-zone loads the overlying fault sufficiently to induce coseismic slip (Fig. 10).

In summary, we can explain the observations of clustering and anticlustering we have made in the Apennines by appealing only to stress interactions between faults and their underlying shear-zones, and between neighbouring fault/shear-zone structures, without including least-work, annealing and/or fluid interactions, or rate and state friction. Therefore, we suggest that stress interactions must be the first order control on temporal clustering of surface faulting earthquakes in our examples because we can explain our observations without appealing to other processes. Annealing, fluid interactions, and frictional variations are also likely to occur, but we suggest that they may be secondary effects and/or controls, but these hypotheses are challenging to test directly because they require measurements from samples from within actively deforming viscous shear-zones and frictional fault-zones.

6.4. Implications for probabilistic seismic hazard assessment (PSHA)

If the explanations for clusters and anticlusters described above and in Fig. 10 are correct, it would be desirable to include this knowledge of clustering and anticlustering into probabilistic seismic hazard assessment (PSHA). This is because probability estimates for the timing of the next earthquake show a strong dependence on the chosen slip-rate (Fig. 5), and on whether fault activity is ongoing, and whether a cluster is treated as ongoing or over (Salditch et al., 2020). One way to include this in PSHA would be to express the conditional probabilities of a fault/shear-zone structure being in a cluster or an anticluster, or exiting an anticluster. Our results provide the opportunity to do this because we have constrained the distributions of cluster and anticluster durations, and hence their mean values and standard deviations, and also the measured timings of cluster and anticlusters on individual faults. Conditional probabilities of a fault/shear-zone structure being in a cluster or an anticluster could then be used, for example, to decide whether to use the high slip-rate from a cluster or a low slip-rate from an anticluster to calculate an expected earthquake frequency magnitude distribution upon which to base probabilistic calculations of future ground shaking (e.g. see Fig. 5).

As an initial test of the utility of using information on clustering and anticlustering in PSHA, here we compare the results of probability calculations of being in a cluster in the recent to present-day with occurrences of earthquake surface rupture confirmed by the historical record, which is thought to be complete for earthquakes >~Mw 5.8 for the last ~500 years (Roberts et al., 2024; Galadini and Galli, 2000) (Tables 1 and 2). Our approach is to compare the timing and duration of clusters for each of these individual examples with the mean and standard deviations for these parameters measured across the region from all 27 sample sites. For the regional dataset, we assume a normal distribution around the mean cluster duration of 2828 years, with a standard deviation of 1994 years (although see Fig. 7k which shows that the data are not perfectly normally distributed). The probability that a fault/shear-zone structure (*P*) is in a cluster (or anticluster) is given by P = 1-normcdf(Z), where Z represents how many standard deviations from the mean a value lies in a normal distribution (Fig. 11a). Data and calculations for individual faults are shown in Table 1.

The data reveal 12 examples of fault/shear-zones where a rupture has occurred in the last 500 years and we have ^{36}Cl data for these structures. From these 12 examples, 9 were interpreted to be in a cluster from the ^{36}Cl data (75%). These 9 fault/shear-zones also had relatively high probabilities of being in a cluster (a mean probability of 46% ± 27%), compared to fault/shear-zones that did not experience earthquake surface ruptures in the last 500 years (a mean of 24% ± 20%) (Fig. 11 b and 11c). With hindsight, one interpretation could be that for faults interpreted to be in a cluster, high slip-rates characterising clusters should have been used 500 years ago to calculate the expected frequency magnitude distributions, and hence probabilities of future earthquake shaking.

Using the same approach, it is also possible to calculate the probability of being in an anticluster, and also exiting an anticluster, using the

Table 1
Probabilities of a fault being in a cluster.

Fault	Mean cluster duration (kyrs)	STD	Start time of last cluster (ka)	Z	normcdf (Z)	Probability to be in a cluster = 1 - normcdf(Z)	Rupture since 1500 AD?	Interpreted to be in a cluster from 36Cl slip history?	Date of Rupture (years A. D.)	Probability of being in a cluster for faults that have ruptured since 1500 AD and were interpreted to be in a cluster from 36Cl	Probability of being in a cluster for faults that have not ruptured since 1500 AD
Assergi	2828	1994	4400	0.79	0.78	0.22	No				0.22
Barete	2828	1994	2900	0.04	0.51	0.49	Yes	Yes	1703.00	0.49	
Barisciano	2828	1994	15000	6.10	1.00	0.00	No				0.00
Campo Imperatore	2828	1994	4200	0.69	0.75	0.25	No				0.25
Campo Felice	2828	1994	3300	0.24	0.59	0.41	No				0.41
Caporciano	2828	1994	2700	−0.06	0.47	0.53	No				0.53
Colfiorito	2828	1994	5700	1.44	0.93	0.07	Yes	No	1997.00	0.07	
Colle Enzano	2828	1994	1600	−0.62	0.27	0.73	Yes	Yes	2009.00	0.73	
Collebrincioni	2828	1994	5600	1.39	0.92	0.08	No				0.08
Costa Corgnetto	2828	1994	3000	0.09	0.53	0.47	Yes	Yes	1997.00	0.47	
Fiamignano	2828	1994	5000	1.09	0.86	0.14	No				0.14
Frattura	2828	1994	4500	0.84	0.80	0.20	No				0.20
Gioia dei Marsi	2828	1994	2500	−0.16	0.43	0.57	Yes	Yes	1915.00	0.57	
Laga	2828	1994	2200	−0.31	0.38	0.62	Yes	Yes	1639 and 2016	0.62	
Leonessa	2828	1994	3300	0.24	0.59	0.41	No				0.41
Liri	2828	1994	5700	1.44	0.93	0.07	No				0.07
Maiella	2828	1994	13500	5.35	1.00	0.00	Yes	No	1706.00		
Mt d' Ocre	2828	1994	2000	−0.42	0.34	0.66	No				0.66
Parasano	2828	1994	3200	0.19	0.57	0.43	Yes	Yes	1915.00	0.43	
Pescasseroli	2828	1994	4600	0.89	0.81	0.19	No				0.19
Poggio di Roio	2828	1994	16000	6.61	1.00	0.00	No				0.00
Roccacasale	2828	1994	4200	0.69	0.75	0.25	No				0.25
Roccapretruro	2828	1994	1300	−0.77	0.22	0.78	Yes?	Yes	2009?	0.78	
San Sebastiano	2828	1994	3800	0.49	0.69	0.31	Yes	Yes?	1915.00	0.31	
Tre Monti	2828	1994	900	−0.97	0.17	0.83	Yes?	Yes	1915?	0.83	
Mt Vettore	2828	1994	4400	0.79	0.78	0.22	Yes	No	2016.00	0.22	
								Total 9.00	**Total 12.00**		
Average						**0.34**				**0.50**	**0.24**
Std										**0.24**	**0.20**

mean and standard deviation values for anticluster durations, again assuming the data are normally distributed around the mean (see Fig. 7r and s which show the distributions are not perfectly normally distributed). We calculate probabilities of being in an anticluster for the three faults that were interpreted to be in anticluster from the ^{36}Cl data, yet experienced an earthquake in the last 500 years. We also calculate the probabilities of exiting an anticluster, which is the inverse of the probability of being in anticluster once the mean anticluster duration has been achieved (Fig. 11a and d). These three faults are on the NE flank of the Apennines, so we use mean and standard deviation values of 6233 ± 3529 years for anticluster durations (Fig. 7t) (see Table 2 for these values plus an alternative where the mean and standard deviation values for the whole dataset were used). Using the values for the NE flank, the Maiella fault had a relatively low probability of being in an anticluster (14%), and hence a high probability of exiting an anticluster (86%). The high probability of exiting an anticluster is due to the measured 10,000 year long duration of its anticluster compared to the mean anticluster duration for the NE flank of the Apennines 6233 years. With hindsight, for the Maiella fault we suggest that probabilities of future ground shaking should have been considered for both high (cluster) and low (anticluster) slip-rate scenarios, because it had a high probability of exiting an anticluster. Indeed, perhaps this approach should be used for all faults within an anticluster if the worst-case scenario is to be considered. Therefore, for fault/shear-zones ruptured in the last 500 years, 10 out of the 12 examples (83%) were either suggested to be within a cluster by the ^{36}Cl data or exhibited a high probability that they were about to exit an anticluster and hence enter a cluster.

We admit that we do not have a full explanation for the other 2 examples. However, we note that Mt. Vettore fault had been quiescent for up to 4690 years (Galadini and Galli, 2000), so perhaps this exceeds typical anticlusters durations on that particular fault/shear-zone. We also note that the Colfiorito fault has accommodated ~6 m slip in the last ~4 kyrs, and so perhaps we are mistaken, and it is actually within a cluster, despite the indication that there appears to have been no slip in the last ~2000 years (Fig. 4). Moreover, the Colfiorito fault is only 3.5 km from the Costa Corgnetto fault which the ^{36}Cl data suggest was in a cluster (Fig. 6), so perhaps they are part of the same fault/shear-zone structure experiencing a cluster. If these ideas are correct, then the occurrence of all 12 historical ruptures are consistent the differential stress change hypothesis and the approach for probability calculations in this paper. Nonetheless despite the uncertainty of these preliminary results, going forward we suggest that our approach could provide information to help to decide what slip-rate to use when calculating the earthquake frequency-magnitude distribution needed to constrain probabilities of future earthquake shaking. In other words, it could provide information on whether to use slip-rates that characterise clusters or anticlusters (e.g. Fig. 5), providing additional constraints for PSHA.

In summary, the probability calculations in Tables 1 and 2 provide intriguing insights into why particular faults may have ruptured in the last 500 years and hence also why velocity vectors measured with GPS and InSAR show an increase in velocity across the relatively narrow

Table 2
Probabilties of existing an anticluster.

Calculated with mean values for all faults										Calculated mean values for the NE flank for anticlusters									
e.g. Mt Vettore Fault										**e.g. Mt Vettore Fault**									
Mean anticluster duration (years)	STD	Start time of anticluster (years BP)	Z	normcdf (Z)	Probability that a fault is in an anticluster = 1 - normcdf(Z)	Mean anticluster duration (years) divided by 2	Residence time in anticluster in excess of the mean anticluster duration (years)	Use inverse of probability of being in an anticluster not? (Yes if excess value is positive number)	Probability of exiting an anticluster	Mean anticluster duration (years)	STD	Start time of anticluster (years BP)	Z	normcdf(Z)	Probability that a fault is in an anticluster = 1 - normcdf(Z)	Mean anticluster duration (years) divided by 2	Residence time in anticluster in excess of the mean anticluster duration (years)	Use inverse of probability of being in an anticluster not? (Yes if excess value is positive number)	Probability of exiting an anticluster
7088	3290	4100	−0.91	0.18	0.82	3544	556	Yes	0.18	6233	3529	4100	−0.60	0.27	0.73	3116.5	983.5	Yes	0.27
e.g. Maiella Fault										**e.g. Maiella Fault**									
Mean anticluster duration (years)	STD	Start time of anticluster (years BP)	Z	normcdf (Z)	Probability that a fault is in an anticluster = 1 - normcdf(Z)	Mean anticluster duration (years) divided by 2	Residence time in anticluster in excess of the mean anticluster duration (years)	Use inverse of probability of being in an anticluster not? (Yes if excess value is positive number)	Probability of exiting an anticluster	Mean anticluster duration (kyrs)	STD	Start time of anticluster (years BP)	Z	normcdf(Z)	Probability that a fault is in an anticluster = 1 - normcdf(Z)	Mean anticluster duration (years) divided by 2	Residence time in anticluster in excess of the mean anticluster duration (years)	Use inverse of probability of being in an anticluster not? (Yes if excess value is positive number)	Probability of exiting an anticluster
7088	3290	10000	0.89	0.81	0.19	3544	6456	Yes	0.81	6233	3529	10000	1.07	0.86	0.14	3116.5	6883.5	Yes	0.86
e.g. Colfiorito Fault										**e.g. Colfiorito Fault**									
Mean anticluster duration (years)	STD	Start time of anticluster (years BP)	Z	normcdf (Z)	Probability that a fault is in an anticluster = 1 - normcdf(Z)	Mean anticluster duration (years) divided by 2	Residence time in anticluster in excess of the mean anticluster duration (years)	Use inverse of probability of being in an anticluster not? (Yes if excess value is positive number)	Probability of exiting an anticluster	Mean anticluster duration (years)	STD	Start time of anticluster (years BP)	Z	normcdf(Z)	Probability that a fault is in an anticluster = 1 - normcdf(Z)	Mean anticluster duration (years) divided by 2	Residence time in anticluster in excess of the mean anticluster duration (years)	Use inverse of probability of being in an anticluster not? (Yes if excess value is positive number)	Probability of exiting an anticluster
7088	3290	1400	−1.73	0.04	0.96	3544	−2144	Yes	0.04	6233	3529	1400	−1.36950977614055	0.0854199905090472	0.91	3116.5	−1716.5	Yes	0.09

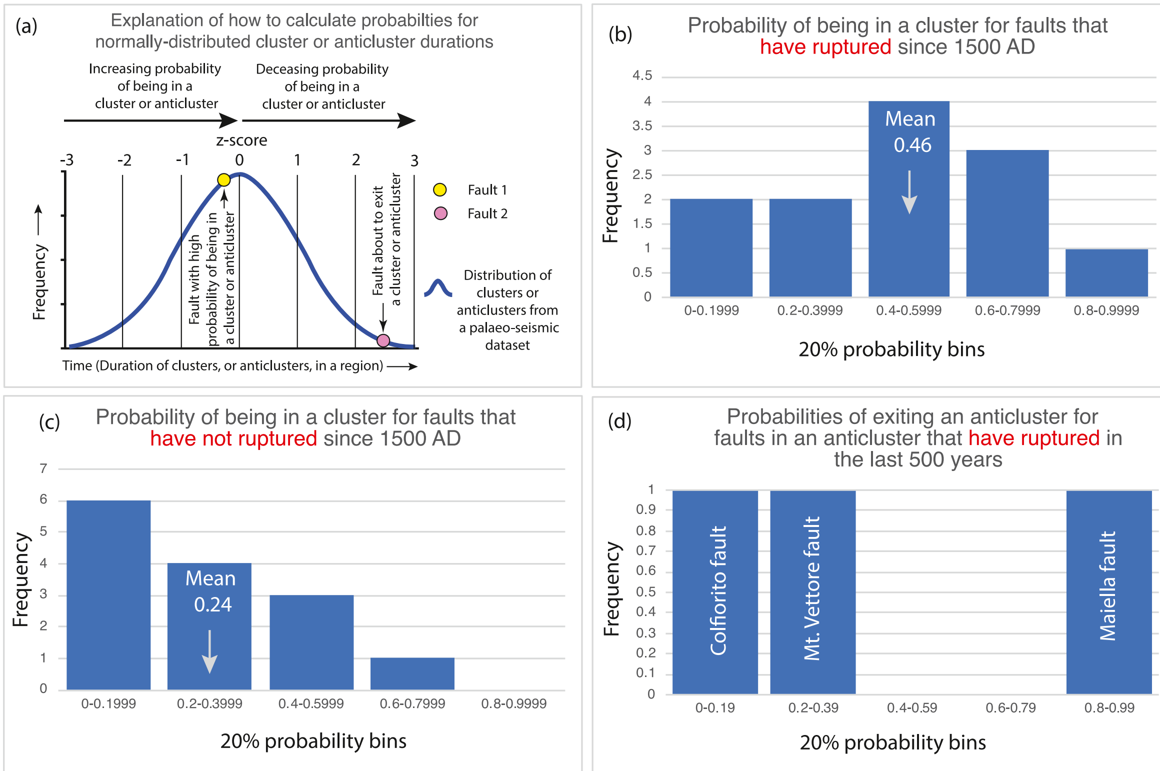

Fig. 11. (a) Probability calculations of a fault being in a cluster or anticluster. (b) and (c) probabilities of being in a cluster for faults that have ruptured since 1500 AD, and have not ruptured since 1500 AD. Calculations in Table 1. (d) Probabilities of a fault exiting an anticluster for faults judged to be in an anticluster (Table 2), yet rupturing in the time period since 1500 A.D. The probability of exiting an anticluster is the inverse of the probability of being in an anticluster once the mean anticluster duration has been achieved. The probabilities indicated in this figure, although preliminary and hence not yet suitable for use in seismic hazard assessment or for use in civil protection, should prompt discussion in these communities about the effects of clustering and anticlustering of surface faulting earthquakes.

region containing the ruptured faults (Fig. 8). Another insight into the seismicity provided herein, is that it appears that some earthquakes that have occurred in the last 500 years in the central Apennines may be examples of earthquakes within clusters, whilst other earthquakes may be examples that terminate an anticluster after a relatively long period of quiescence in seismicity. The probabilities in Tables 1 and 2 are preliminary, and certainly not yet suitable for use in the real world for seismic hazard assessment or civil protection purposes. However, the utility of such probability calculations for clustering and anticlustering needs to be discussed amongst the seismic hazard community, as does the way that this information should be communicated to end-users, but critically, more information on temporal earthquake clustering behaviour is needed from both natural systems and physics based models that include fault to shear-zone interactions and also fault/shear-zone to neighbouring fault/shear-zone interactions.

6.5. *Implications for continental deformation*

Turning to implications for continental tectonics, our findings show that clusters and anticlusters can co-exist in the same fault system, with clusters producing positive stress feedback and clustering along strike associated with in-phase slip, and negative feedback and anticlusters across strike associated with out-of-phase slip (Fig. 12). Moreover, the positions of clusters and anticlusters can fluctuate on a millennial timescale (Electronic Supplement 5; Figs. 6 and 8) and this has important implications for how we should interpret the rheology of the deforming zone. An example is the use of geodetic datasets that attempt to constrain the regional velocity fields and hence the geography and hence rheology and dynamics of the deformation. Geodetic datasets commonly study periods of time lasting a few decades at most and these time periods do not necessarily contain large magnitude surface faulting earthquakes within the studied regional active fault network. Nonetheless, geodetically measured strain-rates have been interpreted as representative of the regional long-term strain-rates because they are thought to constrain the surface expression of deep-seated interseismic deformation on underlying viscous structures. However, to gain the long-term geography of such interseismic deformation this assumes that all the underlying viscous structures are deforming at a constant rate over the long-term. It is suggested herein that, instead, the clusters and anticlusters lasting many millennia indicate that the underlying viscous structures are also undergoing fluctuations in deformation rate that can be higher or lower than the long-term average rate (Roberts et al., 2024). Roberts et al. (2024) suggested this idea of time-varying strain-rate on underlying viscous structures because (a) it is implausible that during anticlusters, the brittle active faults can store increases in differential stress exceeding 100 MPa, along with the elastic strains such stresses would induce, without rupture in large magnitude earthquakes, and (b) during clusters, when many metres of surface slip can accumulate, it is implausible to suggest that underlying viscous shear-zones would not also accommodate similar anomalously large strains and hence strain-rates, due to strain compatibility arguments (Fig. 2c; Cowie et al., 2013; Mildon et al., 2022). In turn, we suggest that millennial timescale variations in strain-rates on individual fault/shear-zone structures within a fault/shear-zone network would produce time-varying spatial patterns of strain-rate measured over decadal timescales (e.g. geodetic timescales) if they could be measured over different decadal time periods. This produces uncertainty in the width of the deforming zone that should be chosen to calculate the rheology of the deforming lithosphere if for example one chose to consider the deformation as a continuum (e.g. England and Molnar, 1997) as opposed to narrow zones of localised

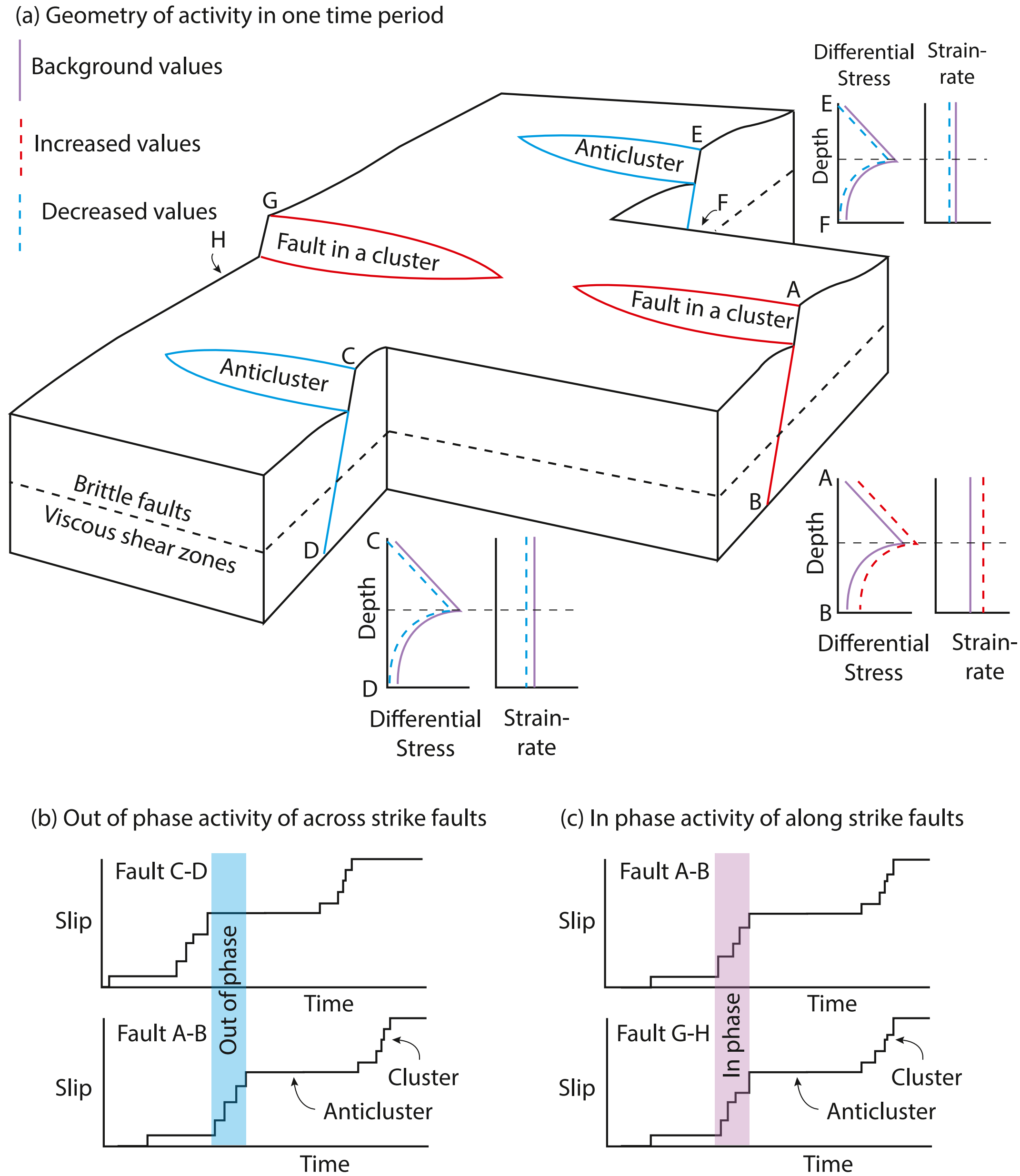

Fig. 12. Summary of stress/strain relationships for active normal fault systems with temporal earthquake clustering.

deformation (e.g. Cowie et al., 2013; Moore and Parsons, 2015). This suggests that strain-rate patterns measured with geodetic approaches should not simply be interpreted in terms of representing the long-term strain-rates, and hence the long-term mechanical/rheological properties of the lithosphere. Instead, the insights provided by ^{36}Cl should be interpreted in terms of the millennial timescale variations in the position, rates and rheology of the deformation that is an inherent part of the dynamics of interacting systems of fault/shear-zones.

7. Conclusions

We present a^{36}Cl dataset for central Italy that constrains slip versus time over tens of millennia for 27 sites along active normal fault/shear-zones,12 of which have not been previously published, and these along with an additional 6 previously-published sites have not been modelled with the code presented by Beck et al. (2018). We also present stress-modelling results that we suggest can explain both the initiation and termination of temporal earthquake clusters and anticlusters, whereas our previous papers have mainly restricted interpretations to the initiation of anticlusters. Our conclusions are as follows.

1) Measurements of the concentrations of ^{36}Cl from fault planes exhumed by fault slip in earthquakes can be used to measure the regional characteristics of slip-rate variability, and earthquake clustering and anticlustering.
2) Slip-rates vary on millennial timescales producing fluctuating widths for the actively-deforming zone.
3) We suggest that the stress increase on an underlying shear-zone produced by coseismic slip on its overlying fault could be the mechanism that initiates an earthquake cluster. The increased strain-rate on the shear-zone after the overlying earthquake will in turn increase the stress on the overlying fault (Fig. 10), leading to positive feedback and repeated re-rupture of the overlying fault. The measured increase in slip-rate on the brittle fault, i.e. the slip-rate enhancement (SRE), matches that predicted for the underlying shear-zone by the dislocation creep flow law. In summary, we suggest that the initiation of a cluster and its continuation through time are caused by earthquakes increasing the differential stress on their

underlying shear-zones followed by positive feedback between shear-zone slip, upwards stress transfer, earthquake slip, and downwards stress transfer.

4) We suggest that stress reductions on shear-zones from coseismic and interseismic slip located across strike could be the mechanism that controls the nature of earthquake anticlusters. The positive stress feedback and repeated re-rupture of a fault in a cluster progressively reduces the stress on fault/shear-zones across strike, placing them into anticlusters, but they are still active and building up to failure which eventually terminates an anticluster, in turn reducing stress across strike, and starting this cycle on a neighbouring structure.
5) Thus, there is feedback both up and down dip between faults and their underlying shear-zones and crucially across strike between neighbouring fault/shear-zone structures. The observations of clustering and anticlustering we have made with ^{36}Cl can be explained by a combination of stress interactions that occur both up and down dip between faults and underlying shear-zones, and across strike in systems of neighbouring fault/shear-zones.
6) If the characteristics and causes of clustering and anticlustering are constrained, observations of these phenomena should be included in probabilistic seismic hazard assessments (PSHA), and also in interpretations of regional deformation rates and crustal rheologies based on geodetic data. Clustering and anticlustering should gain more prominence in discussion within those scientific communities.

CRediT authorship contribution statement

Roberts G.P: Writing – review & editing, Writing – original draft, Visualization, Validation, Project administration, Methodology, Investigation, Funding acquisition, Formal analysis, Data curation, Conceptualization. **Iezzi F:** Writing – review & editing, Writing – original draft, Investigation, Formal analysis, Conceptualization. **Sgambato C:** Writing – review & editing, Writing – original draft, Methodology, Investigation, Formal analysis, Conceptualization. **Robertson J:** Writing – review & editing, Methodology, Conceptualization. **Beck J:** Writing – review & editing, Software, Methodology, Investigation, Formal analysis, Conceptualization. **Mildon Z.K:** Writing – review & editing, Software, Methodology, Investigation, Formal analysis, Conceptualization. **Papanikolaou I:** Writing – review & editing, Methodology, Investigation, Data curation, Conceptualization. **Michetti A.M:** Writing – review & editing, Methodology, Conceptualization. **Faure Walker J.P:** Writing – review & editing, Methodology, Investigation, Conceptualization. **Mitchell S:** Writing – review & editing, Conceptualization. **Meschis M:** Writing – review & editing, Methodology, Conceptualization. **Shanks R:** Methodology, Investigation, Funding acquisition, Formal analysis, Data curation. **Phillips R:** Methodology, Investigation, Formal analysis, Data curation, Conceptualization. **McCaffrey K.J.W:** Methodology, Investigation, Funding acquisition, Formal analysis, Data curation, Conceptualization. **Vittori E:** Writing – review & editing, Validation, Conceptualization. **Visini F:** Writing – review & editing, Methodology, Conceptualization. **Iqbal M:** Investigation, Data curation.

Declaration of competing interest

The authors declare that they have no known competing financial interests or personal relationships that could have appeared to influence the work reported in this paper.

Acknowledgements

Patience Cowie contributed to many discussions that helped the development of the ideas and approaches adopted in this paper. We also thank John McCloskey for his discussions about earthquake science. Bruno Pace and Davide D'Amato are thanked for helping sample the San Sebastiano and Maiella faults and for discussions. Paolo Boncio and Alberto Pizzi are thanked for helping sample the Roccasasale site and for discussions. Leo Zijerveld, Steve Binnie, Klaus Wilcken and Tibor Dunai are thanked for helping sample several faults and discussions. Andrew Watson is thanked for helping with fieldwork. Laura Gregory is thanked for contributing to fieldwork and field sampling, initial discussions, conducting some of the ^{36}Cl chemistry prior to AMS, and compiling the AMS data. Luke Wedmore is thanked for help with fieldwork, LiDAR and GPR studies, and for initial discussions. We thank two anonymous reviewers for their helpful comments that improved the manuscript. NERC Grants NE/E01545X/1, NE/I024127/1, NE/J016497/1 and NE/V012894/1 all helped to fund this study. Full access to the NERC/BGS data repository is available at https://www.bgs.ac.uk/services/ngdc/accessions/index.html#item128345.

Appendix A. Supplementary data

Supplementary data to this article can be found online at https://doi.org/10.1016/j.jsg.2025.105391.

Data availability

All the data are available at the NERC repository https://www.bgs.ac.uk/services/ngdc/accessions/index.html#item128345

References

Allison, K.L., Dunham, E.M., 2018. Earthquake cycle simulations with rate-and-state friction and power-law viscoelasticity. Tectonophysics 733, 232–256.
Angster, S.J., Wesnousky, S.G., Figueiredo, P.M., Owen, L.A., Hammer, S.J., 2019. Late Quaternary slip rates for faults of the central Walker Lane (Nevada, USA): spatiotemporal strain release in a strike-slip fault system. Geosphere 15 (5), 1460–1478.
Barchi, M., Minelli, G., Magnani, B., Mazzotti, A., 2003. Line CROP 03: northern apennines. Mem. Descr. Carta Geol. d'It 62, 127–136.
Beck, J., Wolfers, S., Roberts, G.P., 2018. Bayesian earthquake dating and seismic hazard assessment using chlorine-36 measurements (BED v1). Geosci. Model Dev. (GMD) 11 (11), 4383–4397.
Benedetti, L., Finkel, R., King, G., Armijo, R., Papanastassiou, D., Ryerson, F.J., Flerit, F., Farber, D., Stavrakakis, G., 2003. Motion on the Kaparelli fault (Greece) prior to the 1981 earthquake sequence determined from ^{36}Cl cosmogenic dating. Terra Nova 15 (2), 118–124.
Benedetti, L., Finkel, R., Papanastassiou, D., King, G., Armijo, R., Ryerson, F., Farber, D., Flerit, F., 2002. Post-glacial slip history of the Sparta fault (Greece) determined by 36Cl cosmogenic dating: evidence for non-periodic earthquakes. Geophys. Res. Lett. 29 (8), 87-1.
Benedetti, L., Manighetti, I., Gaudemer, Y., Finkel, R., Malavieille, J., Pou, K., Arnold, M., Aumaitre, G., Bourlès, D., Keddadouche, K., 2013. Earthquake synchrony and clustering on Fucino faults (Central Italy) as revealed from *in situ* ^{36}Cl exposure dating. J. Geophys. Res. Solid Earth 118 (9), 4948–4974.
Biemiller, J., Lavier, L., 2017. Earthquake supercycles as part of a spectrum of normal fault slip styles. J. Geophys. Res. Solid Earth 122 (4), 3221–3240.
Boncio, P., Brozzetti, F., Ponziani, F., Barchi, M., Lavecchia, G., Pialli, G., 1998. Seismicity and extensional tectonics in the northern Umbria-Marche Apennines. Mem. Soc. Geol. It 52 (539), 55.
Bosi, C., 1975. Osservazioni preliminari su faglie probabilmente attive nell'Appennino centrale. Boll. Soc. Geol. Ital. 94 (4), 827–859.
Brozzetti, F., Boncio, P., Lavecchia, G., Pace, B., 2009. Present activity and seismogenic potential of a low-angle normal fault system (Città di Castello, Italy): Constraints from surface geology, seismic reflection data and seismicity. Tectonophysics 463 (1–4), 31–46.
Bubeck, A., Wilkinson, M., Roberts, G.P., Cowie, P.A., McCaffrey, K.J.W., Phillips, R., Sammonds, P., 2015. The tectonic geomorphology of bedrock scarps on active normal faults in the Italian Apennines mapped using combined ground penetrating radar and terrestrial laser scanning. Geomorphology 237, 38–51.
Cavinato, G.P., De Celles, P.D., 1999. Extensional basins in the tectonically bimodal central Apennines fold-thrust belt, Italy: response to corner flow above a subducting slab in retrograde motion. Geology 27 (10), 955–958.
Cello, G., Mazzoli, S., Tondi, E., Turco, E., 1997. Active tectonics in the central Apennines and possible implications for seismic hazard analysis in peninsular Italy. Tectonophysics 272 (1), 43–68.
Chiaraluce, L., Valoroso, L., Piccinini, D., Di Stefano, R., De Gori, P., 2011. The anatomy of the 2009 L'Aquila normal fault system (central Italy) imaged by high resolution foreshock and aftershock locations. J. Geophys. Res. Solid Earth 116 (B12).
Cinti, F.R., Pantosti, D., Lombardi, A.M., Civico, R., 2021. Modeling of earthquake chronology from paleoseismic data: insights for regional earthquake recurrence and earthquake storms in the Central Apennines. Tectonophysics 816, 229016.
Clark, D., McPherson, A., Cupper, M., Collins, C.D.N., Nelson, G., 2017. The Cadell Fault, southeastern Australia: a record of temporally clustered morphogenic seismicity in a

low-strain intraplate region. Geological Society, London, Special Publications 432 (1), 163–185.
Collettini, C., De Paola, N., Holdsworth, R.E., Barchi, M.R., 2006. The development and behaviour of low-angle normal faults during Cenozoic asymmetric extension in the Northern Apennines, Italy. J. Struct. Geol. 28 (2), 333–352.
Cooke, M.L., Toeneboehn, K., Hatch, J.L., 2020. Onset of slip partitioning under oblique convergence within scaled physical experiments. Geosphere 16 (3), 875–889.
Coppersmith, K.J., 1988. Temporal and spatial clustering of earthquake activity in the central and eastern United States. Seismol Res. Lett. 59 (4), 299–304.
Cowie, P.A., Roberts, G.P., 2001. Constraining slip rates and spacings for active normal faults. J. Struct. Geol. 23 (12), 1901–1915.
Cowie, P.A., Roberts, G.P., Mortimer, E., 2007. Strain localization within fault arrays over timescales of 10^0–10^7 Years: observations, explanations, and debates. Dahlem workshop reports. In: Handy, Mark R., Hirth, Greg, Hovius, Niels (Eds.), Tectonic Faults: Agents of Change on a Dynamic Earth. By Gloria Custance. The MIT Press. https://doi.org/10.7551/mitpress/6703.001.0001. ISBN electronic: 9780262274845 Publication date: 2007.
Cowie, P.A., Roberts, G.P., Bull, J.M., Visini, F., 2012. Relationships between fault geometry, slip rate variability and earthquake recurrence in extensional settings. Geophys. J. Int. 189 (1), 143–160.
Cowie, P.A., Phillips, R.J., Roberts, G.P., McCaffrey, K., Zijerveld, L.J.J., Gregory, L.C., Faure Walker, J., Wedmore, L.N.J., Dunai, T.J., Binnie, S.A., Freeman, S.P.H.T., 2017. Orogen-scale uplift in the central Italian Apennines drives episodic behaviour of earthquake faults. Sci. Rep. 7 (1), 44858.
Cowie, P.A., Scholz, C.H., Roberts, G.P., Faure Walker, J.P., Steer, P., 2013. Viscous roots of active seismogenic faults revealed by geologic slip rate variations. Nat. Geosci. 6 (12), 1036–1040.
Cowie, P.A., Underhill, J.R., Behn, M.D., Lin, J., Gill, C.E., 2005. Spatio-temporal evolution of strain accumulation derived from multi-scale observations of Late Jurassic rifting in the northern North Sea: a critical test of models for lithospheric extension. Earth Planet Sci. Lett. 234 (3–4), 401–419.
D'Agostino, N., Mantenuto, S., D'Anastasio, E., Giuliani, R., Mattone, M., Calcaterra, S., Gambino, P., Bonci, L., 2011. Evidence for localized active extension in the central Apennines (Italy) from global positioning system observations. Geology 39 (4), 291–294.
Daout, S., D'Agostino, N., Pathier, E., Socquet, A., Lavé, J., Doin, M.P., Riesner, M., Benedetti, L., 2023. Along-strike variations of strain partitioning within the Apennines determined from large-scale multi-temporal InSAR analysis. Tectonophysics 867, 230076.
Dawson, T.E., McGill, S.F., Rockwell, T.K., 2003. Irregular recurrence of paleoearthquakes along the central Garlock fault near El Paso Peaks, California. J. Geophys. Res. Solid Earth 108 (B7).
Doglioni, C., 1993. Some remarks on the origin of foredeeps. Tectonophysics 228 (1–2), 1–20.
Dolan, J.F., Bowman, D.D., Sammis, C.G., 2007. Long-range and long-term fault interactions in Southern California. Geology 35 (9), 855–858.
Dolan, J.F., McAuliffe, L.J., Rhodes, E.J., McGill, S.F., Zinke, R., 2016. Extreme multi-millennial slip rate variations on the Garlock fault, California: strain super-cycles, potentially time-variable fault strength, and implications for system-level earthquake occurrence. Earth Planet Sci. Lett. 446, 123–136.
Dolan, J.F., Van Dissen, R.J., Rhodes, E.J., Zinke, R., Hatem, A.E., McGuire, C., Langridge, R.M., Grenader, J.R., 2024. One tune, many tempos: faults trade off slip in time and space to accommodate relative plate motions. Earth Planet Sci. Lett. 625, 118484.
DuRoss, C.B., Personius, S.F., Crone, A.J., Olig, S.S., Hylland, M.D., Lund, W.R., Schwartz, D.P., 2016. Fault segmentation: new concepts from the Wasatch fault zone, Utah, USA. J. Geophys. Res. Solid Earth 121 (2), 1131–1157.
Ellis, S., Stöckhert, B., 2004. Elevated stresses and creep rates beneath the brittle-ductile transition caused by seismic faulting in the upper crust. J. Geophys. Res. Solid Earth 109 (B5).
Elston, H., Cooke, M., Hatem, A., 2022. Non-steady-state slip rates emerge along evolving restraining bends under constant loading. Geology 50 (5), 532–536.
EMERGEO Working Group, 2010. Evidence for surface rupture associated with the Mw 6.3 L'Aquila earthquake sequence of April 2009 (central Italy). Terra Nova 22 (1), 43–51.
England, P., McKenzie, D., 1982. A thin viscous sheet model for continental deformation. Geophys. J. Int. 70 (2), 295–321.
England, P., Molnar, P., 1997. Active deformation of Asia: from kinematics to dynamics. Science 278 (5338), 647–650.
Faure Walker, J.P., Roberts, G.P., Cowie, P.A., Papanikolaou, I., Michetti, A.M., Sammonds, P., Wilkinson, M., McCaffrey, K.J.W., Phillips, R.J., 2012. Relationship between topography, rates of extension and mantle dynamics in the actively-extending Italian Apennines. Earth Planet Sci. Lett. 325, 76–84.
Faure Walker, J., Boncio, P., Pace, B., Roberts, G., Benedetti, L., Scotti, O., Visini, F., Peruzza, L., 2021. Fault2SHA Central Apennines database and structuring active fault data for seismic hazard assessment. Sci. Data 8 (1), 87.
Finetti, I.R., Boccaletti, M., Bonini, M., Del Ben, A., Geletti, R., Pipan, M., Sani, F., 2001. Crustal section based on CROP seismic data across the North tyrrhenian–northern apennines–adriatic Sea. Tectonophysics 343 (3–4), 135–163.
Galadini, F., Galli, P., 2000. Active tectonics in the central Apennines (Italy)-input data for seismic hazard assessment. Nat. Hazards 22 (3), 225.
Galadini, F., Messina, P., 2004. Early–middle pleistocene eastward migration of the abruzzi apennine (central Italy) extensional domain. J. Geodyn. 37 (1), 57–81.
Galadini, F., Ricci, G., Falcucci, E., Panzieri, C., 2018. Archaeoseismological evidence of past earthquakes in Rome (fifth to ninth century AD) used to quantify dating uncertainties and coseismic damage. Nat. Hazards 94 (1), 319–348.
Galli, P.A.C., Naso, J.A., 2009. Unmasking the 1349 earthquake source (southern Italy): paleoseismological and archaeoseismological indications from the Aquae Iuliae fault. J. Struct. Geol. 31 (2), 128–149.
Ganev, P.N., Dolan, J.F., Blisniuk, K., Oskin, M., Owen, L.A., 2010. Paleoseismologic evidence for multiple Holocene earthquakes on the Calico fault: implications for earthquake clustering in the Eastern California shear-zone. Lithosphere 2 (4), 287–298.
Gold, R.D., Cowgill, E., 2011. Deriving fault-slip histories to test for secular variation in slip, with examples from the Kunlun and Awatere faults. Earth Planet Sci. Lett. 301 (1–2), 52–64.
Goodall, H.J., Gregory, L.C., Wedmore, L.N., McCaffrey, K.J.W., Amey, R.M.J., Roberts, G.P., Shanks, R.P., Phillips, R.J., Hooper, A., 2021. Determining histories of slip on normal faults with bedrock scarps using cosmogenic nuclide exposure data. Tectonics 40 (3) e2020TC006457.
Gori, S., Falcucci, E., Ladina, C., Marzorati, S., Galadini, F., 2017. Active faulting, 3-D geological architecture and Plio-Quaternary structural evolution of extensional basins in the central Apennine chain, Italy. Solid Earth 8 (2), 319–337.
Gosse, J.C., Phillips, F.M., 2001. Terrestrial in situ cosmogenic nuclides: theory and application. Quat. Sci. Rev. 20 (14), 1475–1560.
Grapes, R.H., Holdgate, G.R., 2014. Earthquake clustering and possible fault interactions across Cook Strait, New Zealand, during the 1848 and 1855 earthquakes. N. Z. J. Geol. Geophys. 57 (3), 312–330.
Hatem, A.E., Gold, R.D., Briggs, R.W., Scharer, K.M., Field, E.H., 2021. STEPS: slip time earthquake path simulations applied to the San Andreas and Toe Jam Hill faults to redefine geologic slip rate uncertainty. G-cubed 22 (10) e2021GC009848.
Hirth, G., Teyssier, C., Dunlap, J.W., 2001. An evaluation of quartzite flow laws based on comparisons between experimentally and naturally deformed rocks. Int. J. Earth Sci. 90, 77–87.
Iezzi, F., Roberts, G., Faure Walker, J., Papanikolaou, I., Ganas, A., Deligiannakis, G., Beck, J., Wolfers, S., Gheorghiu, D., 2021. Temporal and spatial earthquake clustering revealed through comparison of millennial strain-rates from ^{36}Cl cosmogenic exposure dating and decadal GPS strain-rate. Sci. Rep. 11 (1), 23320.
Kastelic, V., Burrato, P., Carafa, M.M., Basili, R., 2017. Repeated surveys reveal nontectonic exposure of supposedly active normal faults in the central Apennines, Italy. J. Geophys. Res.: Earth Surf. 122 (1), 114–129.
King, G.C., Stein, R.S., Lin, J., 1994. Static stress changes and the triggering of earthquakes. Bull. Seismol. Soc. Am. 84 (3), 935–953.
Klinger, Y., Avouac, J.P., Dorbath, L., Karaki, N.A., Tisnerat, N., 2000. Seismic behaviour of the dead Sea fault along araba valley, Jordan. Geophys. J. Int. 142 (3), 769–782.
Klinger, Y., Le Béon, M., Al-Qaryouti, M., 2015. 5000 yr of paleoseismicity along the southern Dead Sea fault. Geophys. J. Int. 202 (1), 313–327.
Lavecchia, G., Boncio, P., Brozzetti, F., De Nardis, R., Visini, F., De Nardis, R., 2011. The contribution of structural geology and regional tectonics to the definition of large-scale seismotectonic provinces and individual seismogenic sources: application to the extensional belt of central Italy. In: Recent Progress on Earthquake Geology. Nova Science Publishers.
Lavecchia, G., Adinolfi, G.M., de Nardis, R., Ferrarini, F., Cirillo, D., Brozzetti, F., De Matteis, R., Festa, G., Zollo, A., 2017. Multidisciplinary inferences on a newly recognized active east-dipping extensional system in Central Italy. Terra Nova 29 (1), 77–89.
Lavecchia, G., Bello, S., Andrenacci, C., Cirillo, D., Ferrarini, F., Vicentini, N., de Nardis, R., Roberts, G., Brozzetti, F., 2022. QUaternary fault strain INdicators database-QUIN 1.0-first release from the Apennines of central Italy. Sci. Data 9 (1), 204.
Lefevre, M., Klinger, Y., Al-Qaryouti, M., Le Béon, M., Moumani, K., 2018. Slip deficit and temporal clustering along the Dead Sea fault from paleoseismological investigations. Sci. Rep. 8 (1), 4511.
Marco, S., Stein, M., Agnon, A., Ron, H., 1996. Long-term earthquake clustering: a 50,000-year paleoseismic record in the Dead Sea Graben. J. Geophys. Res. Solid Earth 101 (B3), 6179–6191.
Maschio, L., Ferranti, L., Burrato, P., 2005. Active extension in Val d'Agri area, Southern Apennines, Italy: implications for the geometry of the seismogenic belt. Geophys. J. Int. 162 (2), 591–609.
Mechernich, S., Reicherter, K., Deligiannakis, G., Papanikolaou, I., 2023. Tectonic geomorphology of active faults in Eastern Crete (Greece) with slip rates and earthquake history from cosmogenic 36Cl dating of the Lastros and Orno faults. Quat. Int. 651, 77–91.
Mechernich, S., Schneiderwind, S., Mason, J., Papanikolaou, I.D., Deligiannakis, G., Pallikarakis, A., Binnie, S.A., Dunai, T.J., Reicherter, K., 2018. The seismic history of the Pisia fault (eastern Corinth rift, Greece) from fault plane weathering features and cosmogenic 36Cl dating. J. Geophys. Res. Solid Earth 123 (5), 4266–4284.
Michele, M., Chiaraluce, L., Di Stefano, R., Waldhauser, F., 2020. Fine-scale structure of the 2016–2017 Central Italy seismic sequence from data recorded at the Italian National Network. J. Geophys. Res. Solid Earth 125 (4) e2019JB018440.
Mildon, Z.K., Roberts, G.P., Faure Walker, J.P., Beck, J., Papanikolaou, I., Michetti, A.M., Toda, S., Iezzi, F., Campbell, L., McCaffrey, K.J., Shanks, R., 2022. Surface faulting earthquake clustering controlled by fault and shear-zone interactions. Nat. Commun. 13 (1), 7126.
Mirabella, F., Brozzetti, F., Lupattelli, A., Barchi, M.R., 2011. Tectonic evolution of a low-angle extensional fault system from restored cross-sections in the Northern Apennines (Italy). Tectonics 30 (6).
Mitchell, S.G., Matmon, A., Bierman, P.R., Enzel, Y., Caffee, M., Rizzo, D., 2001. Displacement history of a limestone normal fault scarp, northern Israel, from cosmogenic 36Cl. J. Geophys. Res. Solid Earth 106 (B3), 4247–4264.

Moore, J.D., Parsons, B., 2015. Scaling of viscous shear-zones with depth-dependent viscosity and power-law stress–strain-rate dependence. Geophys. J. Int. 202 (1), 242–260.
Mozafari, N., Özkaymak, Ç., Tikhomirov, D., Ivy-Ochs, S., Alfimov, V., Sözbilir, H., Schlüchter, C., Akçar, N., 2021. Seismic activity of the manisa fault zone in western Turkey constrained by cosmogenic 36Cl dating. Geosciences 11 (11), 451.
Mozafari, N., Tikhomirov, D., Sumer, Ö., Özkaymak, Ç., Uzel, B., Yeşilyurt, S., Ivy-Ochs, S., Vockenhuber, C., Sözbilir, H., Akçar, N., 2019. Dating of active normal fault scarps in the Büyük Menderes Graben (western Anatolia) and its implications for seismic history. Quat. Sci. Rev. 220, 111–123.
Nijman, W., 1971. Tectonics of Velino-Sirente area, Abruzzi, central Italy - modification of compressional structures by subsequent dilatation and collapse. Proc. K. Ned. Akad. Wet. Ser. B Phys. Sci. 74 (2), 156.
Oskin, M., Perg, L., Shelef, E., Strane, M., Gurney, E., Singer, B., Zhang, X., 2008. Elevated shear-zone loading rate during an earthquake cluster in eastern California. Geology 36 (6), 507–510.
Pace, B., Bocchini, G.M., Boncio, P., 2014. Do static stress changes of a moderate-magnitude earthquake significantly modify the regional seismic hazard? Hints from the L'Aquila 2009 normal-faulting earthquake (Mw 6.3, central Italy). Terra Nova 26 (6), 430–439.
Pace, B., Visini, F., Peruzza, L., 2016. FiSH: MATLAB tools to turn fault data into seismic-hazard models. Seismol Res. Lett. 87 (2A), 374–386.
Palumbo, L., Benedetti, L., Bourlès, D., Cinque, A., Finkel, R., 2004. Slip history of the Magnola fault (Apennines, Central Italy) from ^{36}Cl surface exposure dating: evidence for strong earthquakes over the Holocene. Earth Planet Sci. Lett. 225 (1–2), 163–176.
Peach, B.N., Horne, J., Gunn, W., Clough, C.T., Hinxman, L., Cadell, H.M., 1888. Report on the recent work of the geological Survey in the North-west highlands of scotland, based on the field-notes and maps: (read april 25, 1888.). Quarterly Journal of the Geological Society 44 (1–4), 378–441.
Phillips, T.B., Jackson, C.A., Bell, R.E., Duffy, O.B., Fossen, H., 2016. Reactivation of intrabasement structures during rifting: a case study from offshore southern Norway. J. Struct. Geol. 91, 54–73.
Pialli, G., Alvarez, W., 1995. Chapter B2 Tectonic setting of the miocene northern apennines: the problem of contemporaneous compression and extension. In: Developments in Palaeontology and Stratigraphy, 15. Elsevier, pp. 167–185.
Piccardi, L., Gaudemer, Y., Tapponnier, P., Boccaletti, M., 1999. Active oblique extension in the central Apennines (Italy): evidence from the Fucino region. Geophys. J. Int. 139 (2), 499–530.
Reston, T.J., 1990. The lower crust and the extension of the continental lithosphere: kinematic analysis of BIRPS deep seismic data. Tectonics 9 (5), 1235–1248.
Roberts, G.P., Michetti, A.M., 2004. Spatial and temporal variations in growth rates along active normal fault systems: an example from the Lazio–Abruzzo Apennines, central Italy. J. Struct. Geol. 26 (2), 339–376.
Roberts, G.P., Sgambato, C., Mildon, Z.K., Iezzi, F., Beck, J., Robertson, J., Papanikolaou, I., Michetti, A.M., Walker, J.F., Meschis, M., Shanks, R., 2024. Spatial migration of temporal earthquake clusters driven by the transfer of differential stress between neighbouring fault/shear-zone structures. J. Struct. Geol. 181, 105096.
Rockwell, T.K., Lindvall, S., Herzberg, M., Murbach, D., Dawson, T., Berger, G., 2000. Paleoseismology of the johnson valley, kickapoo, and homestead valley faults: clustering of earthquakes in the eastern California shear-zone. Bull. Seismol. Soc. Am. 90 (5), 1200–1236.
Rolandone, F., Bürgmann, R., Nadeau, R.M., 2004. The evolution of the seismic-aseismic transition during the earthquake cycle: constraints from the time-dependent depth distribution of aftershocks. Geophys. Res. Lett. 31 (23).
Salditch, L., Stein, S., Neely, J., Spencer, B.D., Brooks, E.M., Agnon, A., Liu, M., 2020. Earthquake supercycles and long-term fault memory. Tectonophysics 774, 228289.
Savage, J.C., Burford, R.O., 1973. Geodetic determination of relative plate motion in central California. J. Geophys. Res. 78 (5), 832–845.
Schlagenhauf, A., Gaudemer, Y., Benedetti, L., Manighetti, I., Palumbo, L., Schimmelpfennig, I., Finkel, R., Pou, K., 2010. Using *in situ* Chlorine-36 cosmonuclide to recover past earthquake histories on limestone normal fault scarps: a reappraisal of methodology and interpretations. Geophys. J. Int. 182 (1), 36–72.
Schlagenhauf, A., Manighetti, I., Benedetti, L., Gaudemer, Y., Finkel, R., Malavieille, J., Pou, K., 2011. Earthquake supercycles in Central Italy, inferred from 36Cl exposure dating. Earth Planet Sci. Lett. 307 (3–4), 487–500.
Schmid, S.M., 1982. Microfabric studies as conditions of deformation mechanisms and flow laws operative in mountain building. In: Hsu, K.J. (Ed.), Mountain Building Processes. Academic Press, London, 95-I 10.
Scholz, C.H., 2010. Large earthquake triggering, clustering, and the synchronization of FaultsLarge earthquake triggering, clustering, and the synchronization of faults. Bull. Seismol. Soc. Am. 100 (3), 901–909.
Selvaggi, G., 1998. Spatial distribution of horizontal seismic strain in the Apennines from historical earthquakes. Ann. Geofisc. 41 (2), 241–251.
Serva, L., Blumetti, A.M., Michetti, A.M., 1988. Gli effetti sul terreno del terremoto del Fucino (13.01. 1915); tentativo di interpretazione della evoluzione tettonica recente di alcune strutture. Memor. Soc. Geol. Ital. 35, 893–907.
Shimamoto, T., Noda, H., 2014. A friction to flow constitutive law and its application to a 2-D modeling of earthquakes. J. Geophys. Res. Solid Earth 119 (11), 8089–8106.
Sibson, R.H., 1977. Fault rocks and fault mechanisms. J. Geol. Soc. 133 (3), 191–213.
Sieh, K., Stuiver, M., Brillinger, D., 1989. A more precise chronology of earthquakes produced by the San Andreas fault in southern California. J. Geophys. Res. Solid Earth 94 (B1), 603–623.
Sonder, L.J., England, P.C., 1989. Effects of a temperature-dependent rheology on large-scale continental extension. J. Geophys. Res. Solid Earth 94 (B6), 7603–7619.
Stein, R.S., 2003. Earthquake conversations. Sci. Am. 288 (1), 72–79.
Tesson, J., Benedetti, L., 2019. Seismic history from *in situ* ^{36}Cl cosmogenic nuclide data on limestone fault scarps using Bayesian reversible jump Markov chain Monte Carlo. Quat. Geochronol. 52, 1–20.
Tikhomirov, D., Amiri, N.M., Ivy-Ochs, S., Alfimov, V., Vockenhuber, C., Akçar, N., 2019. Fault Scarp Dating Tool-a MATLAB code for fault scarp dating using in-situ chlorine-36 supplemented with datasets of Yavansu and Kalafat faults. Data Brief 26, 104476.
Tondi, E., 2000. Geological analysis and seismic hazard in the central Apennines (Italy). J. Geodyn. 29 (3–5), 517–533.
Trepmann, C.A., Stöckhert, B., Dorner, D., Moghadam, R.H., Küster, M., Röller, K., 2007. Simulating coseismic deformation of quartz in the middle crust and fabric evolution during postseismic stress relaxation—an experimental study. Tectonophysics 442 (1–4), 83–104.
Tucker, G.E., McCoy, S.W., Whittaker, A.C., Roberts, G.P., Lancaster, S.T., Phillips, R., 2011. Geomorphic significance of postglacial bedrock scarps on normal-fault footwalls. J. Geophys. Res.: Earth Surf. 116 (F1).
Valentini, A., Visini, F., Pace, B., 2017. Integrating faults and past earthquakes into a probabilistic seismic hazard model for peninsular Italy. Nat. Hazards Earth Syst. Sci. 17 (11).
Verdecchia, A., Pace, B., Visini, F., Scotti, O., Peruzza, L., Benedetti, L., 2018. The role of viscoelastic stress transfer in long-term earthquake cascades: insights after the central Italy 2016–2017 seismic sequence. Tectonics 37 (10), 3411–3428.
Vezzani, L., Festa, A., Ghisetti, F.C., 2010. Geology and Tectonic Evolution of the Central-Southern Apennines, Italy, 469. Geological Society of America.
Villani, F., Civico, R., Pucci, S., Pizzimenti, L., Nappi, R., De Martini, P.M., the Open Emergeo Working Group, 2018. A database of the coseismic effects following the 30 October 2016 Norcia earthquake in Central Italy. Sci. Data 5 (1), 1–11.
Vittori, E., Deiana, G., Esposito, E., Ferreli, L., Marchegiani, L., Mastrolorenzo, G., Michetti, A.M., Porfido, S., Serva, L., Simonelli, A.L., Tondi, E., 2000. Ground effects and surface faulting in the September–October 1997 Umbria–Marche (Central Italy) seismic sequence. J. Geodyn. 29 (3–5), 535–564.
Wechsler, N., Rockwell, T.K., Klinger, Y., 2018. Variable slip-rate and slip-per-event on a plate boundary fault: the Dead Sea fault in northern Israel. Tectonophysics 722, 210–226.
Wedepohl, K.H., 1995. The composition of the continental crust. Geochem. Cosmochim. Acta 59 (7), 1217–1232.
Wells, D.L., Coppersmith, K.J., 1994. New empirical relationships among magnitude, rupture length, rupture width, rupture area, and surface displacement. Bull. Seismol. Soc. Am. 84 (4), 974–1002.
Wesnousky, S.G., 2008. Displacement and geometrical characteristics of earthquake surface ruptures: issues and implications for seismic-hazard analysis and the process of earthquake rupture. Bull. Seismol. Soc. Am. 98 (4), 1609–1632.
Wilkinson, M.W., McCaffrey, K.J., Jones, R.R., Roberts, G.P., Holdsworth, R.E., Gregory, L.C., Walters, R.J., Wedmore, L., Goodall, H., Iezzi, F., 2017. Near-field fault slip of the 2016 Vettore Mw 6.6 earthquake (Central Italy) measured using low-cost GNSS. Sci. Rep. 7 (1), 4612.
White, S.H., Burrows, S.E., Carreras, J., Shaw, N.D., Humphreys, F.J., 1980. On mylonites in ductile shear-zones. J. Struct. Geol. 2, 175–187.
Zerathe, S., Lebourg, T., Braucher, R., Bourlès, D., 2014. Mid-Holocene cluster of large-scale landslides revealed in the Southwestern Alps by ^{36}Cl dating. Insight on an Alpine-scale landslide activity. Quat. Sci. Rev. 90, 106–127.
Zygouri, V., Koukouvelas, I., Ganas, A., Tsimi, C., 2023. Clustering of earthquakes along the Pidima-Anthia normal fault: new data from palaeoseismology and tectonic geomorphology and their significance on the earthquake's regularity and recurrence across southern Greece. J. Struct. Geol. 176, 104974.